Evaluation of Four Remote Sensing Algorithms ~~Evaluation of remote sensing algorithms for~~ in E~~e~~stimating A~~a~~ctual E~~e~~vapotranspiration in A~~a~~gricultural E~~e~~nvironments

Phathutshedzo Eugene Ratshiedana [1, 2] Mohamed A. M. Abd Elbasit [3], Elhadi Adam[1] and Johannes George Chirima [2, 4]

[1]School of Geography, Archaeology and Environmental Studies, University of the Witwatersrand, Johannesburg Private Bag x3, Wits, Johannesburg 2050, South Africa
[2]Agricultural Research Council−Natural Resources and Engineering−South Africa, 600 Belvedere Street, Arcadia, Pretoria 0083, South Africa
[3]~~Department of Physical and Earth Sciences, School of Natural and Applied Sciences~~Arid Region Water Research Centre, Sol Plaatje University, Kimberley 8301~~0~~, South Africa
[4]Department of Geography, Geoinformatics and Meteorology, University of Pretoria, Pretoria 0028, South Africa

Correspondence to: Phathutshedzo Eugene Ratshiedana (Ratshiedanap@arc.agric.za)

Abstract. Accurate estimation of actual evapotranspiration (ETa) at both field and larger spatial scales is crucial for understanding crop water use and hydrological interactions particularly in regions facing water scarcity. In South Africa, ETa data gaps hinder effective agricultural water management. Advances in geospatial techniques combining Geographical Information Systems (GIS) and remote sensing have made it possible to estimate ETa over large areas. However, the reliability of this depends on the accuracy of algorithms used which must be validated against ground measurements. With the lack of direct ETa measurements in South Africa, this has been a challenging task. This study evaluated ETa variability at farm level to the level of an irrigation Scheme, covering over 36,000 hectares. A total of 22 Landsat 8 satellite images from 2019 to 2021 were used to estimate ETa based on four algorithms: the Surface Energy Balance Algorithm for Land (SEBAL), Surface Energy Balance System (SEBS), Vegetation Index (VI)-based ETa and Crop Water Stress Index (CWSI)-based ETa. Field-scale estimates were compared ~~to measurements from a smart field weighing lysimeter, while~~ and validated using a smart field weighing lysimeter while the algorithms estimates were evaluated at irrigation-scheme scale using weather-station-based extrapolation.~~larger-scale~~~~values at weather station location farms across the irrigation scheme~~ ~~estimates were validated against using~~ ~~extrapolated ETa values~~ ~~from the field lysimeter and weather station~~ ~~.~~ The VI-based algorithm performed best, with r = 0.92, R^2 = 0.85 and the lowest errors (RMSE = 0.58 mm d^{-1}; MAE = 0.44 mm d^{-1}), followed closely by SEBAL (r = 0.92, R^2 = 0.84, RMSE = 0.83 mm d^{-1}, MAE = 0.69 mm d^{-1}). The SEBS algorithm showed moderate performance, while CWSI performed poorly.~~The SEBAL, SEBS and VI-based ETa algorithms correlated well with field-scale lysimeter data, while the CWSI-based algorithm showed poor correlation. SEBAL emerged as the best-performing algorithm, with high correlation coefficients (r=0.91–0.96), strong R² values (0.83–0.92) and the lowest errors (RMSE 0.31–0.89 mm d⁻¹, MAE 0.27–0.82 mm d⁻¹).~~ ~~Most importantly~~While SEBAL is the second best performing algorithm, the validation of VI-ETa approach in estimating

ETa against lysimeter measurements demonstrated its reliability with strong correlations and low error metrics, as a result, the VI-ETa algorithm is a computationally efficient alternative. The uncertainty analysis indicated that extrapolated ETa estimates were reliable within ±7–12%. The study demonstrates the potential use of some remote sensing algorithms for~~of~~ accurate ETa estimation to support ~~better~~ irrigation scheduling, which may lead to reduced water overuse, in water-scarce environments.

1 Introduction

Evapotranspiration (ET) is a critical component in hydrological studies representing a combination process encompassing evaporation of soil water content, water from other land cover surfaces, canopy interception, and losses though transpiration from vegetation canopy (Pandey et al., 2016; Raza et al., 2022). In agricultural settings, actual evapotranspiration (ETa) serves as a crucial measure for quantifying crop water use, ~~this component reflects the actual water use in real-world~~ which can be ~~obtained through field measurements~~derived from lysimeter mass balance measurements which include changes of mass due to changes in soil moisture variability (Djaman et al., 2023). Accurate quantification of ETa in irrigated environments allows farmers to determine the amount of water that has been used by crops after irrigation for precise irrigation scheduling (Elfarkh et al., 2022; Djaman et al., 2023). In irrigation schedules where ETa is not quantified, the likelihood is that farmers will either over-irrigate or under-irrigate (Abd Elbasit and Ratshiedana, 2024)~~Mndela et al., 2023)~~. The overuse of water in irrigation contributes largely to the continuous depletion of the available scarce water resources (Mabhaudhi et al., 2021; Du Plessis, 2023). In alternate scenarios, crops might suffer water logging conditions and salinity problems, which can impact crop yields negatively (Ingrao et al., 2023).

Monitoring and managing agricultural water resources requires accurate measurement of ETa, however, this requires expensive devices such as smart field weighing lysimeters and eddy covariance systems which are not practical to deploy across larger extents (Sharma et al., 2015; Djaman et al., 2019). In areas where direct measurement devices are not available, crop evapotranspiration (ETc) is calculated from meteorological measurements using micrometeorological models and standardized Kc values such as those published by the FAO (Allen et al., 1998). The difference between ETc and ETa is that ETa is influenced by the actual field conditions which are determined through actual field measurements while ETc is based on estimations based on standard Kc values. ETc represents how much water the crop would ideally use, whereas, ETa tells represents the actual amount of water that the crop has used~~The difference between ETc and ETa is that ETa is influenced by the actual field conditions which are determined through actual field measurements while ETc is based on estimations based on standard Kc values. ETc represents how much water the crop would ideally use, whereas, ETa tells represent the actual amount of water that the crop has used.~~. For many decades, ~~crop evapotranspiration (~~ETc~~)~~ has been estimated using meteorological methods requiring data acquired from weather stations, this includes studies conducted by Annandale et al. (2002) and by Moeletsi et al. (2013). These stations are still not enough in most parts of South African agricultural landscapes to be representative of field-scale ETc estimation with high accuracy (Ncoyini et al., 2022). According to Ramoelo et al. (2014)

South Africa currently has only two open-access FLUXNET eddy covariance stations, insufficient for national-scale ET validation across heterogeneous agricultural landscapes. The Food and Agriculture Organization (FAO) has provided crop coefficient (Kc) values for a wide range of crops cultivated globally to aid in estimating ETc (Allen et al., 1998). However, the original Kc values were developed outside South Africa and were not specifically tailored for horticultural or non-agricultural vegetation while in agriculture they were not developed using drought-resistant cultivars which of lately are prevalent in the country's arid regions (Mulovhedzi et al., 2020; Mukiibi et al., 2023). According to Allen et al. (1998) ETc can be estimated by multiplying the crop specific Kc values by the reference evapotranspiration (ETo) value. The Kc values are determined as the ratio of ETa to ETo, with ETo calculated using meteorological variables with models like the Penman-Monteith and Dalton amongst others (Dalton, 1802; Allen et al., 1998). ETc represents evapotranspiration from disease-free crops grown under optimal soil water and management conditions (Allen et al., 1998), whereas ETa reflects actual field conditions including water stress. However, ETa on the ground is typically derived using specialized equipment such as lysimeters, although these devices offer high accuracy representation of actual water use, they are point instruments which are limited in their ability to represent the spatial variability of ETa particularly in heterogeneous landscapes (Doležal et al., 2018; McNamara et al., 2021).

ETa estimated under standard conditions such disease-free, well-fertilized crops, grown in large fields, under optimum soil water conditions, and achieving full production under the given climatic conditions ~~With ETa~~ being key in development of Kc values and determining the true reflection of crop water consumption, South Africa faces a substantial gap in the direct measurement of ETa primarily due to the limited availability of the necessary devices for this purpose. This limitation is highlighted in the study of (Meijninger and Jarmain, 2014), who could not validate satellite ET estimates from a remote sensing-based model in Kwazulu-Natal. The country has only two FLUXNET eddy covariance stations providing open-access data, with other stations being privately owned and inaccessible for national water management efforts (Baldocchi et al., 2001; Pastorello et al., 2020~~;Blatchford et al., 2020~~).

Remote sensing offers a practical way to estimate ~~ETa~~ ETa over large areas, given the cost and logistical challenges of ground-based measurements across diverse vegetation (Cai et al., 2021). The use of remote sensing provides an alternative to ground-based measurements which often lack the spatial coverage required for effective water management (Tan et al., 2021; Saha et al., 2022; Tran et al., 2023). However, achieving high accuracy in remote sensing relies on integrating ground-truth measurements obtained through precise instruments and models that can capture the variability across different land cover types(Li et al., 2023; Tran et al., 2023). Satellite-derived ET estimates can be influenced by factors such as cloud cover, atmospheric conditions, sensor saturations and their spatio-temporal resolution (Mckenzie et al., 1998; Wang et al., 2023). In regions with heterogeneous landscapes and variable cropping patterns, these challenges are further exacerbated leading to discrepancies between satellite-derived ET estimates and ETa observed in the field (Lian et al., 2022).

Several ET algorithms have been developed, applied and validated across different environments (Zamani and Rahimzadegan, 2018). These algorithms include the Surface Energy Balance Algorithm for Land (SEBAL), Mapping Evapotranspiration at High Resolution with Internalized Calibration (METRIC), Atmosphere Land Exchange Inverse (ET-ALEXI), Surface Energy Balance (SEBS) model developed by Su (2002) was implemented and the Three-Temperature Model (3T Model) amongst others (Bastiaanssen, 2000; Allen et al., 2007; Yan, 2016). Studies involving the utilization of remote sensing data for assessing water use and hydrology in South Africa have been conducted employing the SEBAL algorithm alongside data from Landsat at different environments (Shoko et al., 2015; Ndou et al., 2018; Singels et al., 2018). These studies reported estimates inaccuracies which they attributed them to low accuracy data which were measured using instruments such as eddy covariance systems which are known to have energy balance closure problems. However, Bastiaanssen et al. (2005) reported that the SEBAL algorithm can have an accuracy of about 85% agreement with measurements at field scale while it can be improved to over 95% if applied at seasonal scale~~across different seasons~~. However, studies focusing on SEBAL seasonality impact are still lacking in South Africa. Gibson et al. (2013) suggested that future research using the SEBS algorithm by Su (2002) in South Africa should focus exclusively on agricultural landscapes. This recommendation arises from the limitations of ET algorithms when applied to a wide range of land use types.

Vegetation index-based evapotranspiration (VI-ETa) approaches have been proven to be effective in estimating ETa across diverse regions. For instance, Glenn et al. (2010) reviewed the combination of ground-based ETa measurements with VI-ETa methods across different biomes obtaining strong correlations with coefficients of determination ranging between 0.45 and 0.95. Their findings indicate correlations between 0.67 and 0.97, with which they suggested that VI-ETa algorithms can be more accurate when calibrated with accurate ground measurements such as those obtained from weighing lysimeters. Jiang et al. (2020) emphasized that errors in ETa estimates can be reduced to within 5% using such devices, while Hunsaker et al. (2005) demonstrated similar precision. Nagler et al. (2013) used MODIS EVI to estimate ETa in riparian and agricultural areas achieving less than 10% error when compared to eddy covariance measurements. They recommended VI-ETa models for drylands where non-vegetative factors are minimal and suggested the Penman-Monteith or Blaney-Criddle methods for areas lacking ETa data. Abbasi et al. (2021) applied VI-ETa using Landsat imagery to monitor agricultural drought in Iran, despite the lack of ground data in the country. They found that VI-ETa estimates correlated well with in-situ data at the basin scale, with errors ranging from 15 to 21%, and from 2.5 to 34% at the country scale. These studies highlight the potential of VI-ETa to accurately estimate crop water use provided accurate calibration data such as data from weighing lysimeters is available. In South Africa, VI-ETa use remains limited due to challenges in obtaining precise ETa measurements for calibration. Furthermore, the use of crop water stress index (CWSI) for determining ETa remains unexplored in the country.

The Vaalharts Irrigation Scheme which is one of the largest in South Africa requires accurate ETa estimation for optimizing water usage and ensuring sustainable agricultural practices. This is because the scheme lacks its own source of water to sustain productivity, ~~however;~~and the scheme depends on water from ~~areas~~ sources such as the Vaal River through the Bloemhof dam to sustain irrigation (Maisela, 2007). Water in the scheme is only monitored from discharge points for billing purposes using flow meters, however, the amount of water used by crops and the surrounding vegetation after each irrigation event remains unknown. These amounts are crucial in irrigation water management particularly for regional water accounting, understanding the crop water demand helps with allocation and long-term sustainability planning. Given the limitations of ETa variability data, there is a pressing need for research focused on evaluating and improving the accuracy of ETa algorithms to support informed decision-making by researchers, irrigation water managers and policymakers.

This study aims at evaluating the capabilities and accuracies of SEBAL, SEBS, VI-based ETa and the CWSI-based ETa algorithms using an integration of a high precision smart field weighing lysimeter and automatic weather stations approach. The specific objectives were: (i) to use ETa measurements by a smart field weighing lysimeter across four cropping seasons to validate estimates from the four algorithms at field scale and, (ii) to extrapolate ETa from lysimetric measurements to extrapolate ETa from lysimetric measurements to other fields within the irrigation scheme that are equipped with weather stations. This is the first study to evaluate remotely sensed ETa using a smart field weighing lysimeter as demonstrated by (Tran et al., 2023) that lysimeter approach in South Africa is uncommon on their review study. This study contributes to the broader field of remote sensing offering more information on the strengths and limitations of these algorithms in diverse agricultural landscapes to solve the irrigation water management and ETa data scarcity challenges.

2 Methods and materials

2.1 Study area description

This study was conducted within the Vaalharts irrigation scheme located in the Northern Cape province of South Africa between the coordinates: 24°44'16.91"E and 27°38'33.23"S on the North, while on the Southern parts the scheme starts at 24°37'37.46"E and 28° 4'54.38"S. The study was conducted from September 2019 until May 2021 capturing different seasons and crops. In 2019, winter barley was planted in the experimental field, while in 2019-2020 summer season, maize was planted. During the 2020 winter season, barley was planted again while in 2020-2021 summer season soybean was planted. The exact location of the experimental lysimeter farm within the irrigation scheme is indicated in Fig. 1a. At this farm, barley, maize, and soybean were grown during the study period (2019–2021). The weather station sites were surrounded mainly by maize, barley and wheat fields although soybeans and groundnuts were also present depending on the season. The irrigation scheme is the largest irrigation scheme in South Africa covering over 36 950 hectares (Ojo et al., 2011). The scheme is located between two plateaus, and its terrain is low-lying, with elevations ranging between 1080 and 1 137 m above sea level (asl). The scheme receives irrigation water through a canal system with water coming from the Bloemhof dam, the dam which is fed by the Vaal River. Additional water comes from the Harts River were water goes into the irrigation scheme facilitated by a diversion weir located in Warrenton town, the weir collects water from the Harts and Bloemhof dam into the scheme. The study area experiences low annual rainfall averaging between 400 and 500 mm year^{-1} (Moeletsi et al., 2022). Several crops are planted including maize, wheat, barley, cotton, soybeans, groundnuts, watermelon and various fruit trees such as pecans and olives (Pretorius, 2018; Ratshiedana, 2022). The soils within the scheme are alluvial soils prone to salinization (Ojo, 2013). Pivot irrigation systems dominate the area, while other forms of irrigation, such as flood irrigation, bubblers, sprinklers and drips, are common (Maisela, 2007; Verwey and Vermeulen, 2011; Ratshiedana, 2022). The irrigation scheme supports both small-scale and large-scale farming operations. The importance of this scheme lies in it being a major source of employment and food security and contributing significantly to the local economy where most agricultural enterprises emerged to support farming and retail was developed to support the farming communities residing around the scheme (Maisela, 2007). The study area comprises of an 18-ha experimental farm and four validation sites with automatic weather stations with station locations named: SABBI, Tadcaster, Jankempdorp and Ganspan (Fig.1).

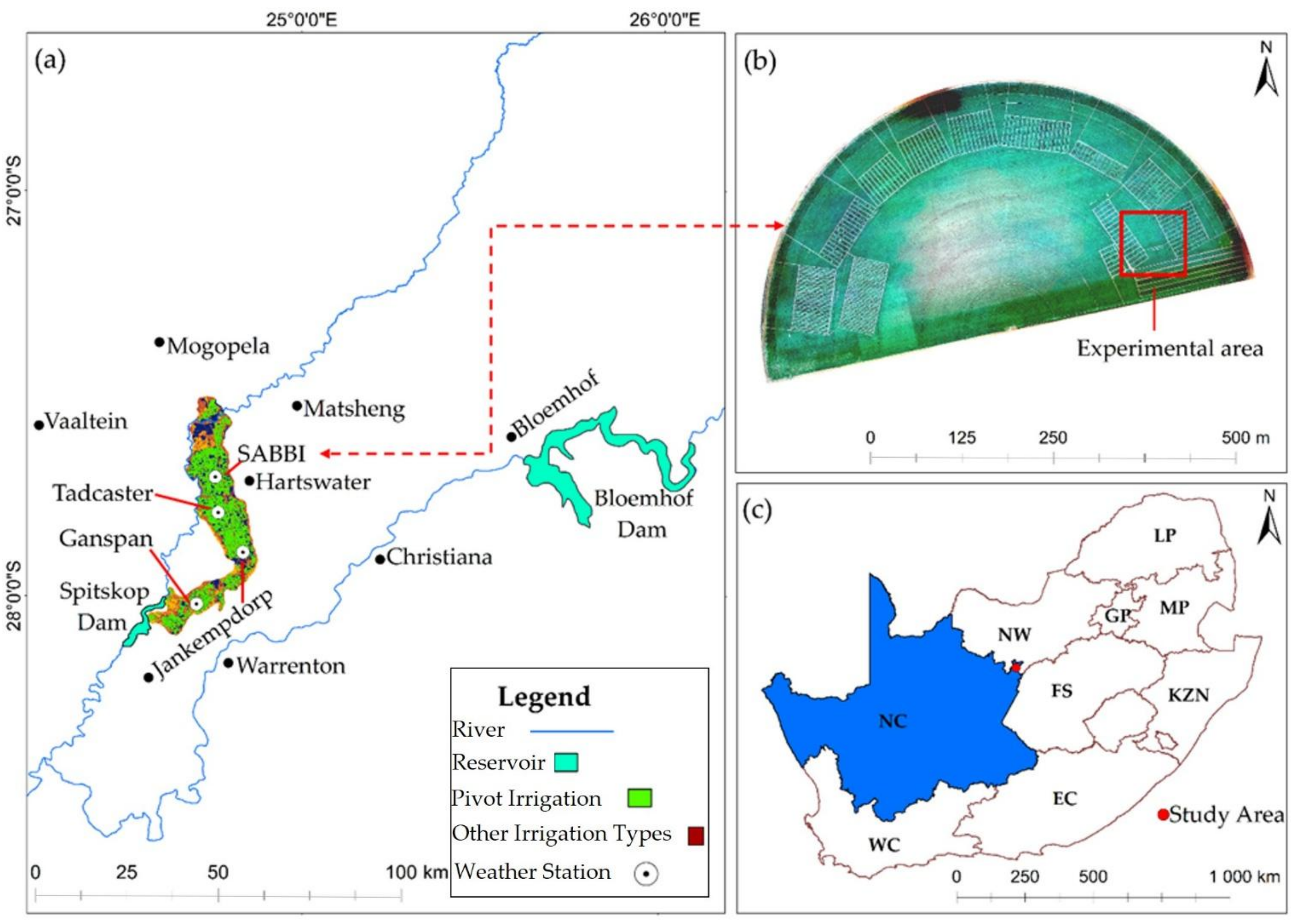

Figure 1. Map showing the study area distinct regions, (a) delineates the Vaalharts irrigation scheme, its surrounding towns, major rivers and dams, (b) shows the (18-ha) experimental farm where ground measurements were installed which is pivot irrigated with uniform crop, and (c) indicates the study area's position in relation to various provinces.

2.2 Study approach

Having identified that direct measurement of ETa in South Africa is the limiting factor in evaluating remote sensing ETa products and algorithms; this study focuses on the use of a smart field weighing lysimeter as an accurate tool for measuring ETa to enable the evaluation and calibration of four ETa algorithms. Ground-based measurement and monitoring techniques were used for validation, while satellite-based monitoring provided a continuous and cost-effective source of information. These measurements ~~developed~~ were used to develop an irrigation scheme scale validation proxy using meteorological information considering the scarcity of data in an agricultural landscape. The research approach is summarised in the conceptual representation below (Fig.2).

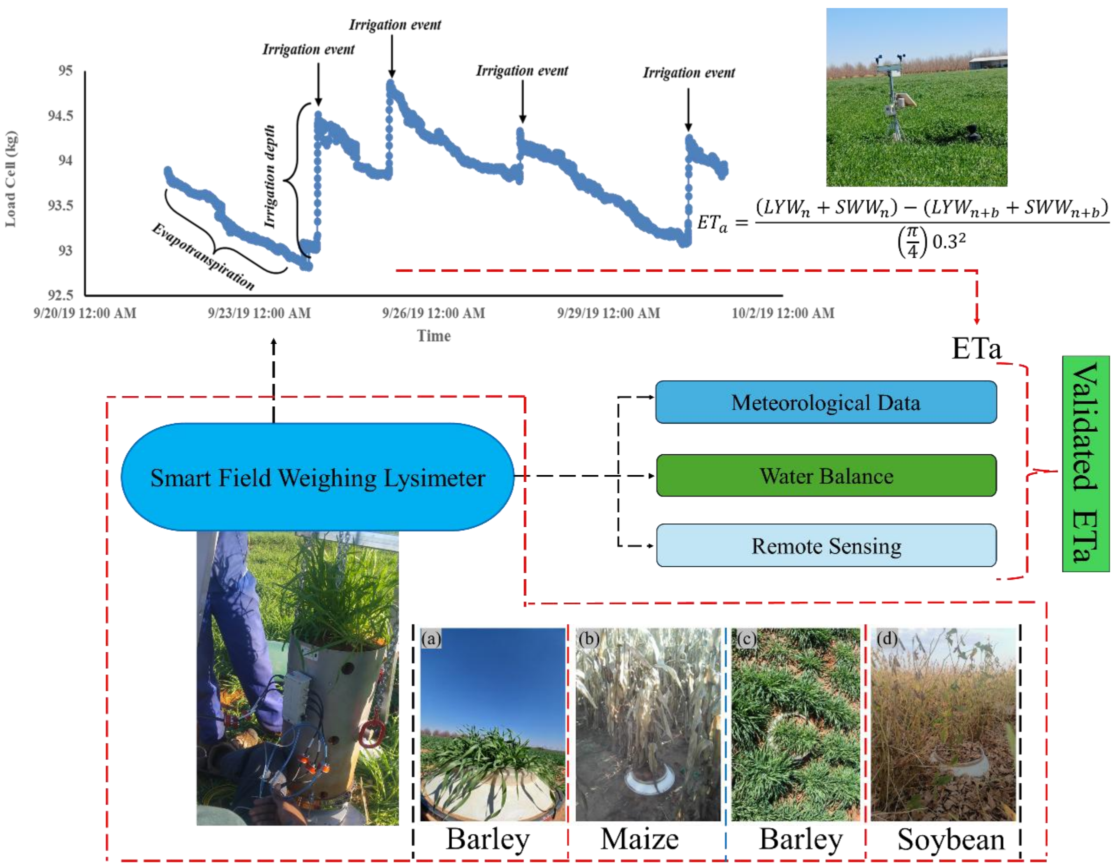

Figure 2. Conceptual framework for the study approach linking satellite data and ground measurements.

2.3 Data Acquisition

2.3.1 Satellite data acquisition and pre-processing

Remotely sensed Landsat 8 images with multiple bands were obtained from the United States Geological Survey (USGS) Earth Explorer portal (https://earthexplorer.usgs.gov/ Accessed: 04 February 2023) using a bulk downloader for automatic and continuous download of the specified data (Table 1). A total of 22 images were acquired for the study period, their cloud cover % are given in Table (S1). The Level 1 Terrain Corrected (L1T) were retrieved covering a period between 1st September 2019 and 31 May 2021. The pre-processing of Level 1 Terrain Corrected (L1TP) data was executed using the Semi-Automatic Classification Plugin (SCP) in QGIS. Radiometric calibration was done to transform digital numbers (DN) to top-of-atmosphere (TOA) reflectance. This conversion was achieved by utilizing the metadata linked to each image file. Since the L1TP data had already been georeferenced, geometric correction was unnecessary. Atmospheric correction was applied to mitigate the impact of atmospheric scattering and absorption. The atmospheric correction was done using the Dark Object Subtraction 1 (DOS1) method (Chakouri et al., 2020). The method assumes that some pixels in the image such as water bodies or shadows should have very low or zero reflectance in some bands, especially in the visible range. These pixels represent dark objects, because of atmospheric scattering; these pixels appear brighter than they should. The DOS1 method subtracts a constant value, which is the assumed atmospheric path radiance from all pixels in each band to correct this atmospheric effect and improve surface reflectance accuracy. For the thermal bands, processing was carried out to derive temperature values in degrees Celsius (°C) while they were resampled using the raster calculator and bilinear resampling method in QGIS to align with the 30 m resolution of multispectral bands.

Table 1. Landsat 8 Satellite Data used for estimating ETa

Band Name	Wavelength
Band 2 - Blue	0.45-0.51 nm
Band 3 - Green	0.53-0.59 nm
Band 4 - Red	0.64-0.67 nm
Band 5 - Near Infrared (NIR)	0.85-0.88 nm
Band 6 - Short-wave Infrared (SWIR) 1	1.57-1.65 nm
Band 7 - Short-wave Infrared (SWIR) 2	2.11-2.29 nm
Band 10 - TIRS 1	10.60-11.19 µm
Band 11 - TIRS 2	11.50-12.51 µm

2.3.2 Lysimeter installation and measurements

A smart field weighing lysimeter by METER Group© was used to measure field soil-water-crop interactions. The lysimeter used is cylindrical in shape with 60 cm height and a diameter of 30 cm with the surface area of 0.07 m^2. During the installation of the lysimeter, a fresh soil sample core was sampled from the tilled field. The soil monolith hosted the field cultivated crop of each season replicating the soil, environmental and treatment conditions of the surrounding field with the crop matching the one planted in the entire farm. Retrieving the soil monolith core from the lysimeter involved the use of three rope straps which were fixed to steel hook anchors embedded in the ground. These straps were used to secure a jack positioned on top of the cylinder which effectively drove the cylinder into the soil. The process continued until a sufficient volume of soil was filled reaching the bottom level within the cylinders. At the base of the lysimeters cylinder the closing process was achieved using gypsum-filled ceramic caps, which contributed to effective sealing. These caps played a significant role in establishing a suitable boundary between the external field environment and the controlled internal environment within the lysimeter. Within the gypsum filled caps, two pumps were secured to maintain the balance in conditions of wetness between the lysimeter and the field condition. Preventive measures against potential leakage included the incorporation of a rubber seal between the cylinder walls and the contact point of the ceramic cap which were further reinforced by a metallic strap to ensure a secure connection. A weighing balance platform was positioned below these caps, secured using metal fasteners and tensioned nut and bolts. This lysimeter contains a suite of sensors which measure soil water content fluxes, soil temperature, matric potential, soil electrical conductivity and contains weighing balances that measure the lysimeter mass and another balance measuring the drainage amount outside the lysimeter cylinder. The weight losses are related to soil water evaporation and crop transpiration, while mass gains are related to irrigation or precipitation events. The lysimeter used offers real-time monitoring and high temporal resolution data at an interval of 1 minute on mass balances, while sensors measurements were done at 10 minutes interval. The process of calculating ETa from smart field weighing lysimeter data was done using R in Posit Software (PBC), formerly known as RStudio (https://posit.co/). The processing was focused on aggregating hourly measurements to daily totals to match with the daily ETa estimated by the satellite images. The *tidyverse* and *lubridate* packages were used to prepare the data by extracting the date component from the timestamp. The daily ETa values were visualized using the *ggplot2* package to identify patterns or anomalies and the results were exported as .csv for further analysis. The exported data was further processed using the Savitzky-Golay filtering technique on Originlab© software to smooth ETa data where un-explainable spikes existed as done by Peters et al. (2014). The filter replaced spike values with smoothed values, which were calculated from the adjacent point values. The filter fitted a polynomial to a moving window of the raw lysimeter data replacing each central point with the predicted value which fitted effectively removing the noise and spikes without distorting the trend on the dataset for each season. Three crops were used during the experimental period between 2019 and 2021. In 2019, winter barley measurements were done between 9th September 2019 and 12th November 2019. During the 2019-2020 season, measurements were done between 14th December 2019 and 6th May 2020. In the 2020 winter season, measurements were made between 7th June 2020 and 13th October 2020 while in 2020-2021 season measurements were between 17th January 2021 and 9th May 202. The lysimeter during each season featured a crop that covered the entire 18-ha experimental field. Evapotranspiration was computed using the changes in lysimeter and drainage balances weight with irrigation and precipitation being negligible because the estimations were done during zero-irrigation and precipitation days based on Eq. (1) and (2), while mean ETa was done based on equation (S8)~~:~~

$$\mathrm{ETa} = \cancel{\mathrm{I} -} \Delta \mathrm{D} - \Delta \mathrm{S} \times 14.14 \tag{1}$$

where ~~ETa I is irrigation or precipitation in mm from the irrigation gauge,~~ ΔD is the change in the lysimeter drainage mass balance in kg ~~whereas,~~and ΔS is the change in lysimeter mass balance (kg).

Based on the measured parameters~~ with different units~~, the above formula can be represented using the simplified Eq. (2):

$$\mathrm{ETa} = (\mathrm{Lm(n)} + \mathrm{Dm(n)} - \mathrm{Lm(n-1)} + \mathrm{Dm(n-1)} \times 14.14 \tag{2}$$

where Lm (n) is the lysimeter mass in kg at time "n", Dm (n) is the drainage mass in kg at time "n", Lm (n−1) is the lysimeter mass at time "n−1", while Dm (n−1) is the drainage mass in kg at time "n−1". The value 14.14 was obtained based on the assumption that, 1 kg of water seepage in the lysimeter equals 0.001 m^3 which when divided by the surface area of the lysimeter it gives 0.014 m which is equivalent to 14 mm, as a result each 1 kg equalled 14 mm.

2.3.3 Meteorological data

An ONSET HOBO remote monitoring system (RX3000) automatic weather station was used to measure all meteorological variables at field level. These variables included air temperature, relative humidity, solar radiation, wind speed, wind direction, rainfall and barometric pressure. Rainfall depth (mm) was measured and aggregated to daily totals and incorporated into the water balance equation alongside irrigation inputs. The operating range of the station is -40 to 60 °C while it does support remote communications with its continuous solar power supply supporting the battery life. The station was configured with different soil sensors including moisture and temperature sensors while it provided cloud-based data access through HOBOlink. The stations used for the purpose of calibration and validation of remotely sensed variables were the automatic weather stations owned by the Agricultural Research Council (ARC) of South Africa. The stations are equipped with humidity sensors, air temperature, wind speed sensors, wind direction, gust sensor, rain gauge, barometric sensors, soil moisture sensors and solar radiation sensors (Moeletsi et al., 2022). Each weather station is installed with windspeed and direction sensors at a height of ~~1.~~2 m as indicated in Moeletsi et al. (2022) who indicated the height of sensors are positioned at 200 cm. The meteorological information is retrieved remotely and can be accessed through: https://www.arc.agric.za/arc−iscw/Pages/Agrometeorology−Reports.aspx accessed on 16 June 2023. For this study, the data required was extracted for the times September 2019 to end of May 2021.

2.4 Remote sensing algorithms

2.4.1 Vegetation Index-Based Evapotranspiration (VI-ETa) estimation

The VI-ET algorithm is a remote sensing technique which is used to estimate ETa by incorporating vegetation indices (VIs) such as the Normalized Difference Vegetation Index (NDVI) given in Equation (S7)~~or Enhanced Vegetation Index (EVI~~) (Glenn et al., 2010). These indices were derived using spectral band ratio and combination methods where reflectance values from specific multispectral bands such as red and near infrared are mathematically combined to represent vegetation properties like health, canopy density and greenness using vegetation index formulas directly to the satellite spectral bands. The algorithm integrates these indices with ETo derived from meteorological data for the purpose of determining Kc values at different vegetation growth stages representing the relationship between vegetation status and water use (Nagler et al., 2013). The vegetation indices serve as proxies for the fractional vegetation cover and leaf area index, which both of which influence transpiration rates. On the other hand, the values of ETo represents the evaporative demand of a hypothetical reference crop under optimal water conditions. The Kc relates actual crop water use to the atmospheric demand. Since the Kc values differ over the crop growth stages reflecting changes in canopy development, vegetation indices derived from remote sensing are used to estimate Kc values. The empirical or semi-empirical models establish linear relationships between vegetation indices and Kc values by calibrating observed ETa from the lysimeter against vegetation index values. The VI-ETa algorithm then estimates ETa by multiplying the VI-based Kc by meteorological derived ETo to enable the modelling of spatially distributed estimates of vegetation water use across different land covers. This algorithm was selected because it links the VIs to Kc values, which removes the complexity of physical modelling or detailed parameterization required by energy balance or surface temperature-based models, which rely on high-quality thermal data and complex calibration. The approach relies on multispectral data to represent the spatial distribution of crop water use. Moreover, this algorithm provides a simple scalable ETa estimates with relatively low computational demand, enabling effective monitoring over large areas with frequent temporal coverage. It is also easier to customize and calibrate the algorithm to specific crop types or land covers using ground data, which can improve its accuracy. The general equation for ETa or ETc which resemble the same component is given by Eq. (3):

$$\mathrm{ETa} = \mathrm{ET_o} \times \mathrm{Kc} \tag{3}$$

The values of Kc were derived at field scale using the FAO procedure (Allen et al., 1998) as the ratio of ETa to ETo using Eq. (4):

$$\mathrm{Kc} = \frac{\mathrm{ET_a}}{\mathrm{ETo}} \tag{4}$$

The ETo which incorporates the variability in weather conditions was determined using R from an automatic weather station data using the standard Penman-Monteith equation introduced by Allen et al. (1998) given as Eq. (5):

$$ET_o = \frac{0.408\Delta(R_n - Go) + \gamma\left(\frac{Cn}{T+273}\right)U_2(e_s - e_a)}{\left(\Delta + \gamma(1 + C_d U_2)\right)} \qquad (5)$$

where the symbol Δ is the slope of saturation vapour pressure (kPa °C^{-1}). The term Rn corresponds to the total radiation on the vegetation surface (MJ m² d^{-1}) over a 24−hour period, while the term G_o denotes the soil heat flux density (W m^{-2}). The average daily air temperature is indicated as T (°C), while the term U_2 is the average hourly wind speed measured at a height of ~~1.~~2 m (m s^{-1}). The variable es denotes the saturation vapour pressure (kPa), while e_a signifies the actual vapour pressure (kPa). The difference of $e_s - e_a$ indicates the saturation vapour pressure deficit (kPa). The term γ is the psychrometric constant (kPa °C^{-1}), whereas Cn and Cd are constants that vary based on the reference crop surface being used (Allen et al., 1998). For this study, Cn was 900 was used, while Cd was 0.~~38~~34, these were selected because they represent a short reference crop while they provide consistency across varying climatic conditions.

The Kc values were determined for every satellite pass date based on the lysimeter measured ETa and the determined ETo at farm level. The measurement of ETa was only based on one farm within the entire irrigation scheme due to limitation of ETa measuring device in the scheme. As a result, the relationship between Kc values and NDVI was used to model the Kc for the entire irrigation scheme using the approach used by Niu et al. (2020) for estimating Kc spatial variability. The determination of Kc was done for four cropping seasons at the farm level resulting in four Kc models which were amalgamated into an ensemble Kc model. The determination of Kc was done on QGIS using the NDVI layer derived from the NIR and the Red band using Eq. (6):

$$Kc = a \times NDVI + b \qquad (6)$$

where a and b are the coefficients from the relationship between NDVI and Kc

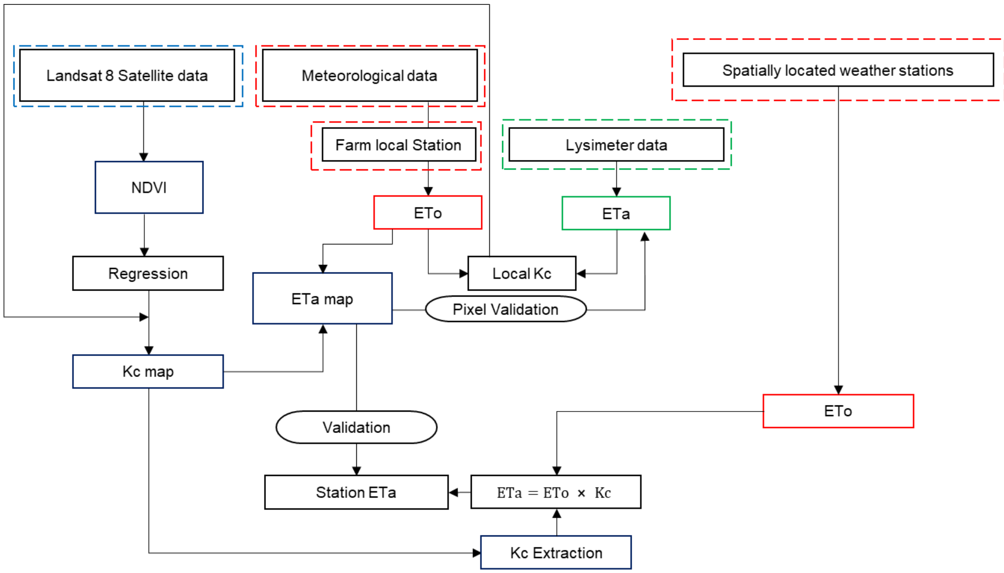

Figure 3. The workflow for VI-ETa algorithm's actual evapotranspiration estimation and validation. The workflow integrates various steps including data processing, generation of the ETa maps and accuracy validation steps.

Since three different crops were used in this study, to account for crop-specific variability in the NDVI–Kc relationships, we developed separate regression models for all three crops using the lysimeter-derived ETa values for each crop cycle see Table S2. Each model captured the phenological dynamics and canopy development which was specific to each crop. These seasonal crop-specific regressions were then compared and combined into an ensemble model by weighting them according to the length and completeness of the measurement periods (Table S2). This was done to ensure that the extrapolation of Kc across the irrigation scheme reflects both the intra-seasonal growth patterns and inter-crop variability, thereby minimizing the bias that would arise from using a single regression relationship across diverse crops.

2.4.2 The SEBAL Model

The Surface Energy Balance Algorithm for Land (SEBAL) is a remote sensing algorithm used to estimate ETa based on thermal and multispectral datasets across large areas by calculating the energy balance of the Earth's surface. This algorithm was developed by Bastiaanssen in the early 2000s with the purpose of using images to analyse the exchange of energy between the land surface and the atmosphere above it to the rate of water losses through evaporation and transpiration (Bastiaanssen, 2000). The retrieval of ETa was based on the energy balance approach using the SEBAL incorporated on the Surface Energy Balance and Crop Water Stress Spatial Analysis (SEBCS) plugin on QGIS. The SEBCS used the specific spectral bands from Landsat8 listed in Table 1 data to derive the biophysical and radiative parameters for estimating ETa. The SEBCS plugin in QGIS implements the SEBAL algorithm as described by Bastiaanssen (1998), allowing for the estimation of ETa using satellite thermal and multispectral data. The SEBAL algorithm is based on the surface energy balance equation, where ETa is calculated as the residual of Rn, G, and H. The plugin automates the derivation of each component wherein: Rn is computed using incoming and outgoing shortwave and longwave radiation, with albedo derived from multispectral reflectance bands. The component, G is estimated empirically using NDVI and surface temperature, while H is calculated through the near-surface temperature gradient and aerodynamic resistance derived from the selection of hot and cold anchor pixels. The plugin uses an iterative approach to link surface temperature to temperature differences and applies default or user-supplied wind data to estimate H. Lastly, the latent heat flux is obtained as the residual energy of Rn – G – H, which is converted to ETa in mm per day using the latent heat of vaporization. The Red and NIR bands were used to calculate NDVI, which helps in estimating the vegetation cover. The blue band, Red, NIR and SWIR to derive the land surface albedo, while the TIRS were used in deriving LST to compute the heat flux. The SEBAL algorithm uses these spectral inputs into the energy balance equation given as Eq. (7):

$$\mathrm{ETa} = \mathrm{Rn} - \mathrm{G_o} \cancel{\mathrm{Go}} - \mathrm{H} \tag{7}$$

where Rn represent the net radiation, G_o is the soil heat flux while H is the sensible heat flux and ETa is the evapotranspiration component equivalent to the latent heat flux (LE), all variables are measured in MJ m^{-2} d^{-1}.

2.4.3 Crop water stress-based ETa

Jackson et al. (1981) established a mathematical relationship between the crop water stress index (CWSI) and the vegetation water consumption. To compute ETa, they devised an approach given as Eq. (8):

$$\mathrm{ETa} = \mathrm{ETo} \times (1 - \mathrm{CWSI}) \tag{8}$$

The same formula was applied in this study using the Landsat 8 thermal data. The CWSI was calculated using the CWSI plugin on QGIS using thermal images, the outputs were multiplied by the sunshine hours for daily CWSI. The CWSI was computed based on Eq. (9):

$$\mathrm{CWSI} = \frac{\Delta \mathrm{T} - \Delta \mathrm{Tm}}{\Delta \mathrm{Tx} - \Delta \mathrm{Tm}} \tag{9}$$

where ΔT represents the difference in air temperature as determined by LST, ΔTm indicates the least change in T_air, and ΔTx denotes the greatest divergence between LST and air temperature. For this purpose, ΔT_m= minimum LST-T_air (proxy for Twet) while ΔT_x= maximum LST-T_air (proxy for Tdry). Twet is approximated by the lowest observed canopy-air temperature difference while Tdry is approximated by the highest observed difference.

$$\Delta \mathrm{T} = \mathrm{a} \times \cancel{\mathrm{T_s}} \mathrm{LST} + \mathrm{b} \tag{10}$$

where a, and *b* are the regression coefficients determined from the anchor pixels, ~~.~~ the hot pixels were identified over dry, bare soil surfaces characterized by high LST and low NDVI values, representing conditions of minimal ET. Cold pixels were selected over dense vegetation areas exhibiting high NDVI and low LST which are indicative of maximum ETa under well-watered conditions. The anchor pixels were selected manually following the standard SEBAL methodology to ensure that they represented the extreme energy balance conditions within each satellite scene.

2.4.4 The ~~Surface Energy Balance~~ SEBS ~~model~~modelling approach

The Surface Energy Balance System (SEBS) was introduced by Su (1999, 2002) for estimating heat flow fluxes and evaporative fractions. This model shares similarities with the SEBAL model, with a distinction being that, the SEBAL model is empirical and relies on anchor pixels from remote sensing datasets, while SEBS is a physically-based model which uses ~~atmospheric theory and requires more~~ weather data including: air temperature, wind speed, relative humidity, incoming solar radiation and incoming longwave radiation.. The soil heat flux was calculated using Eq. (11):

$$G_o = R_n[T_c + (1 - F_{vc})(T_s - T_c)] \tag{11}$$

where Go is the soil heat flux, the term Rn represents the net radiation while Tc stands for the psychrometric constant for the canopy air layer. The variable Ts represents the psychrometric constant for the soil and Fvc is the fractional vegetation cover calculated as:

$$\mathrm{Fvc} = (\mathrm{NDVI} - \frac{\mathrm{NDVI_{min}}}{\mathrm{NDVI_{max}} - \mathrm{NDVI_{min}}})^2 \tag{12}$$

where, NDV_{min} is minimum NDVI and $NDVI_{max}$ is maximum NDVI.

$$T_c = \frac{c_p \times P}{\varepsilon \times \lambda} \tag{13}$$

where Cp is the specific heat of air at constant pressure ≈ 1.013×10^3 (J $kg^{-1} \times$K), P is the atmospheric pressure (kPa), ε is the ratio of molecular weight of water vapor/dry air ≈ 0.622, while λ is the latent heat of vaporization which is approximately: 2.45×10^6 J kg^{-1}.

$$T_s = \gamma - \Delta T \tag{14}$$

where ΔT is a temperature difference from thermal imagery between air and surface.

2.5 The validation of ETa algorithms at field scale

2.5.1 Selection of validation pixels at field and irrigation scheme levels

One pixel was selected were the lysimeter and weather station were located at the experimental farm, the pixel represented estimate values at ~~farm~~ field level from each algorithm. The ETa estimates from the four evaluated algorithms were validated by directly comparing them with daily ETa measurements from a smart field weighing lysimeter over 22 days across different cropping seasons at field scale.. In the study area, only one farm was equipped with the smart field weighing lysimeter. The system could only validate ETa estimated at its location pixel for the four algorithms. However, to validate the effectiveness of the algorithms at different locations within the irrigation scheme, a relationship between Kc developed and ETo was used to estimate ETa using weather station locations, this follows the derivation of ETa by multiplying ETo with Kc. Direct comparisons between estimated ETa and extrapolated ETa were used for the validation process. However, the selection of validation dates were based on the periods when the scheme was entirely green during summer seasons when the area was not under intense water stress. This was to ensure that ETa is evaluated based on an active vegetation pixel than bare soil pixels, which would result in soil water evaporation possibly giving no values in such a water deficit environment and would not comply with the requirements of some modeling schemes such as the CWSI. The spatial assessment was conducted for the models that demonstrated good results at the farm level with the assumption that poor-perfoming algorithms will likely not yield good results when transferred to different environments.

2.5.2 Evaluation metrics

The statistical metrics used for the evaluation process included the correlation coefficient (r), coefficient of determination (R^2), Root Mean Square Error (RMSE), Mean Absolute Error (MAE), Standard Error (SE) and Bias . The error metrics were used to determine the level of errors attributed to the used algorithms on their estimation of ETa compared to the measurements of ETa by the lysimeter. These metrics were selected because each of them captures a unique aspect of model accuracy and reliability. The r and R^2 assess the strength and consistency of the relationship between estimated and measured values, highlighting the model's ability to explain variability. The RMSE and MAE quantify the magnitude of errors, with RMSE emphasizing large deviations and MAE providing an average error magnitude. The bias evaluate the presence of systematic over- or underestimation, offering insights into the directional tendencies of the algorithms. The values of SE reflects the variability of the error distribution between the algorithm-estimated ETa and the lysimeter-measured ETa. A lower SE indicates that the estimates are consistently close to the actual measured values which suggests higher precision. In combination, these metrics ensure a strong evaluation by portraying both precision and accuracy of the algorithms and identifying any systematic discrepancies (Chicco et al., 2021; Hodson, 2022). The complete set of equations used for the evaluation is included in Equations (S1)–(S6).

2.6. Sensitivity analysis approch

The accuracy of ETa estimations which are derived from remote sensing models is influenced by uncertainties in both input data and the structure of the used model. As a result, key input data such as meteorological variables, vegetation indices, and surface energy balance components were derived from a single weather station and satellite imagery over the experimental field. However, although this setup supports high-resolution validation, the extrapolation of ETa across the entire irrigation scheme introduces potential uncertainties. To assess the strength of the results, a sensitivity analysis was conducted to evaluate how perturbations in critical input parameters affect model outputs. For this reason, three ~~representative~~selective input variables that strongly influence ETa estimations were selected. These variables included: T_air which was used in SEBS, CWSI-ETa and VI-ETa. The Rn which was used across all models especially on SEBS and SEBAL as well as NDVI for the SEBAL and VI-ETa approach. Each variable was independently perturbed by ±5% and ±10%, and the resulting percentage change in daily ETa estimates was recorded for each model. The analysis was performed on selected dates representing different crop growth stages and environmental conditions.

3 Results

3.1 Estimation of Kc based on vegetation index (VI) for ETa determination

The variations in Kc and NDVI across four cropping seasons where the lysimeter was installed are illustrated in Fig.4. During the 2019 cropping season (Fig.4−a), the season began with relatively high Kc and NDVI values (0.86 and 0.8), suggesting that the crop was healthy and actively transpiring, with substantial green canopy cover. As the season advanced to around DOY 268, Kc and NDVI values gradually became closer (0.76 and 0.79), indicating consistent vegetation growth and stabilization of canopy greenness. Towards the end of the season (DOY 300), both indices declined to 0.43 and 0.38, reflecting the senescence phase of the crop marked by reduced greenness and water demand. In the 2019−2020 season (Fig.4−b), around DOY 316, both Kc and NDVI values were low (0.41 and 0.37), representing the early growth stage with sparse vegetation and minimal transpiration. The indices reached their peak by DOY 31 in 2020, indicating the height of the crop's growth and greenness, before tapering off again to 0.4 and 0.35 as the season ended, consistent with the crop's natural lifecycle. On other seasons as depicted on Fig. 4−c and Fig. 4−d: Similar trends were observed, wherein Kc and NDVI closely mirrored the crop development stages. During the early stages, the indices remained low, gradually increasing as the crop established its canopy. Peaks are the period of maximum crop growth, followed by declines as the crop matured and approached senescence. A summary of Kc models derived through linear regression analysis between Kc and NDVI are shown in Table (S2), while the scatter plots between estimated ET and measured ETa are shown in Figure (S1).

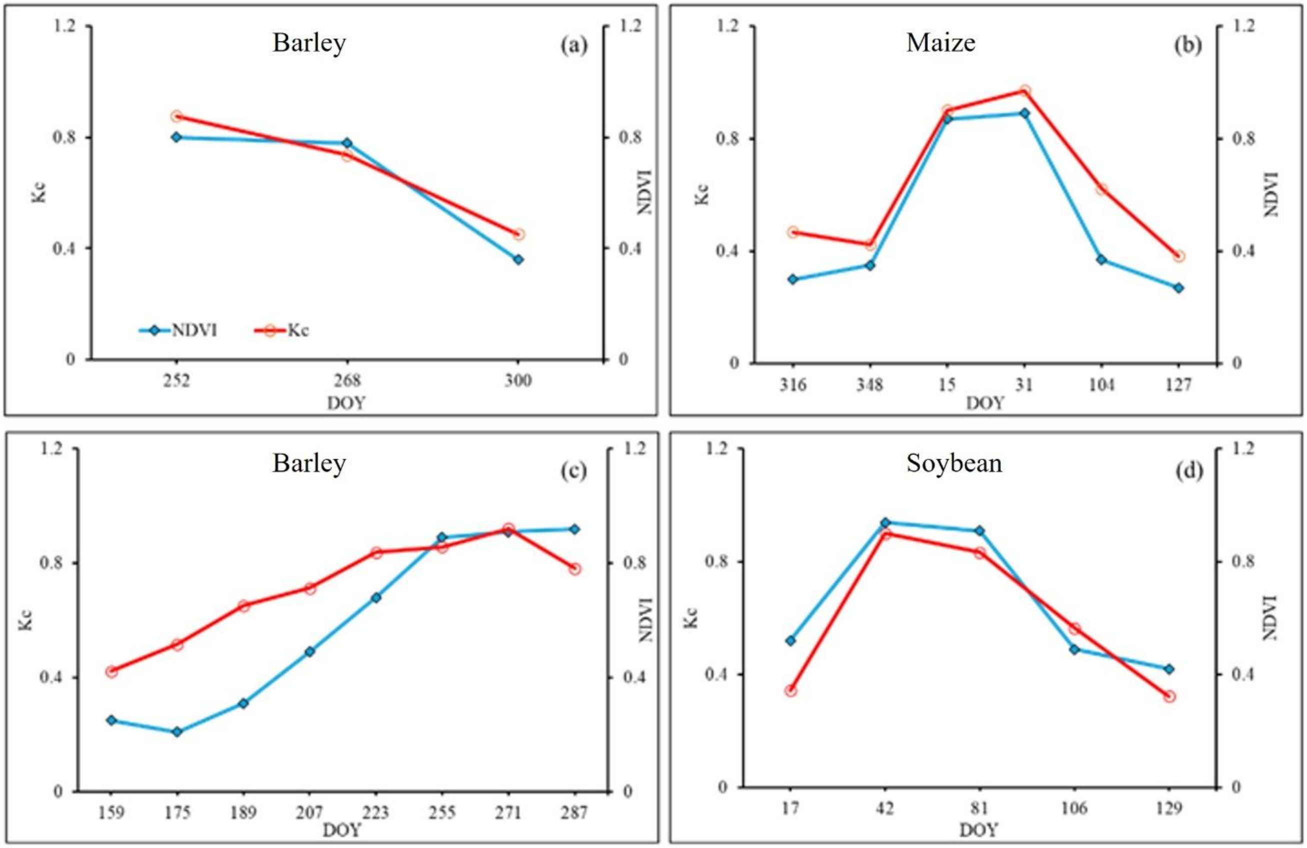

Figure 4. The variability of Kc values in relation to the changes in NDVI for the period 2019−2021 where (a) is the winter cropping season in 2019, (b) relates to 2019−2020 summer season, (c) is the 2020 winter season and (d) is the 2021 summer season calculated in the Southern Hemisphere.

3.2 Evapotranspiration variability across different seasons and algorithms at the experimental site

Figure 5 (a−d) presents the temporal trends between lysimeter ETa and ETa estimated using four algorithms at the field level. Figure 5−a shows the variations between lysimeter ETa and VI-ETa across the cropping seasons. The graphs indicate that, on most days, lysimeter ETa closely matched VI-ETa, with only slight underestimations and overestimations on some days. Overall, the differences were minimal. The VI-based ETa algorithm exhibited the lowest average MAE (0.44 mm d^{-1}) across the four validation sites, followed by SEBAL (0.69 mm d^{-1}), while SEBS showed the highest error (0.87 mm d^{-1}). Figure 5−b compares lysimeter ETa with SEBAL algorithm estimates. Both methods exhibited similar trends, with SEBAL estimates increasing and decreasing in tandem with lysimeter ETa. Throughout the cropping seasons, both methods captured ETa fluxes similarly. However, SEBAL tended to overestimate ETa on most days, with evident overestimations on days of the year (DOY) 31, 130, 207, 287, and 113, and slight underestimations around DOY 320. Across the four validation stations, SEBAL exhibited an average bias of approximately 0.33 mm d^{-1}, indicating a slight tendency to overestimate ETa. In comparison, the VI-based ETa algorithm showed a small negative bias (−0.12 mm d^{-1}), suggesting a slight underestimation of ETa, whereas SEBS displayed a larger positive bias of 0.52 mm d^{-1}, indicating stronger overestimation. Figure 5−c illustrates the relationship between lysimeter ETa and CWSI−ETa. Unlike the other algorithms, CWSI−ETa showed high variability on most days, with values often surpassing those of lysimeter ETa. The lysimeter ETa displayed smoother variability compared to the more fluctuating CWSI−ETa values. Figure 5−d shows that SEBS ETa estimates closely tracked lysimeter ETa values, like the SEBAL and VI-ETa estimates. The scatter plots between the models and lysimeter ETa values is shown in Figure (S1).

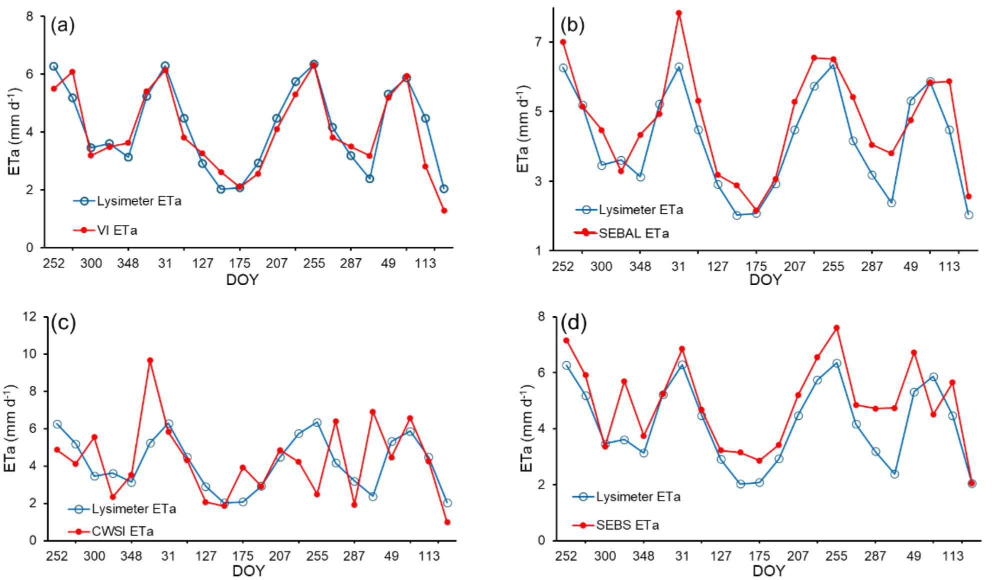

Figure 5. Variability of lysimeter ETa and estimated ETa by VI ETa (a), SEBAL (b), CWSI ETa (c) and SEBS (d) algorithms.

Figure 6 shows a comparison of the total ETa estimates from 2019 to 2021 which was a total of 22 days of cloud free Landsat 8 data across the four different algorithms: SEBAL, SEBS, VI-ETa, and CWSI-ETa against lysimeter-measured ETa in millimetres (mm). The total estimated ETa for each algorithm is represented by a bar in the corresponding colour. The lysimeter data acts as a benchmark of ETa, and differences in bar heights demonstrates how closely each algorithm aligns with the measured ETa. This reflection provides insight into the accuracy and reliability of the algorithms in estimating ETa over the study period. The total ETa measured by the lysimeter which matches the evaluated Landsat 8 images was 91.63 mm while SEBAL had a closer reading with only 1.41 mm. VI-based ETa followed with 2.36 mm which was followed by the SEBS algorithm with 5.63 mm difference whereas the CWSI-based ETa algorithm had the biggest difference of 16.24 mm over the evaluated period. These findings demonstrate the reliability of SEBAL, VI-based ETa and SEBS in accurately estimating ETa.

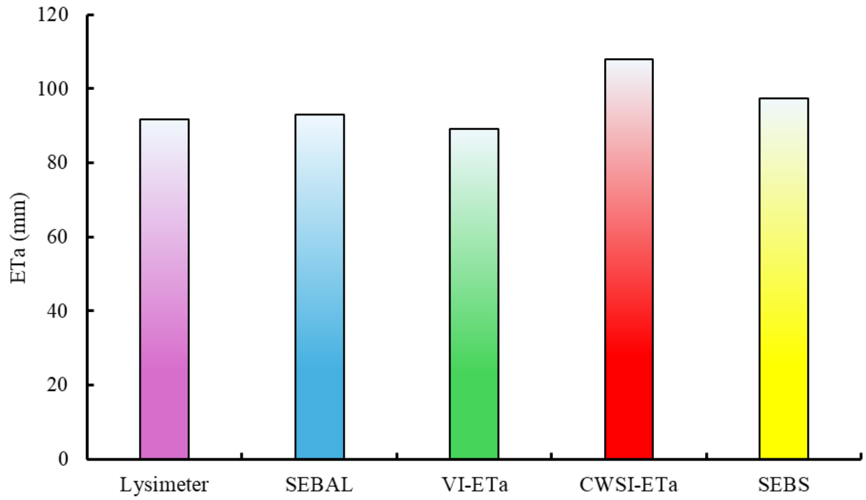

Figure 6. Total lysimeter measured and estimated ETa by SEBAL (blue), VI-ETa (green), CWSI (red) and SEBS (yellow) during the study period.

3.3 Summary of evaluation metrics for the four algorithms against the smart lysimeter at field scale

The evaluation of SEBAL, VI, CWSI and SEBS ETa algorithms against lysimeter quantified ETa using statistical performance metrics revealed clear differences in their predictive capabilities (Fig. 7). The SEBAL and VI algorithms demonstrated the strongest agreement with lysimeter ETa values, with both models achieving a high correlation coefficient ($r = 0.92$) and coefficients of determination (R^2) of 0.84 and 0.85 respectively. In addition, these two methods produced the lowest error statistics, confirming their superior predictive accuracy. The VI model showed the lowest errors, with an RMSE of 0.58 mm d^{-1} and MAE of 0.44 mm d^{-1}, followed by the SEBAL algorithm which produced an RMSE of 0.83 mm d^{-1} and MAE of 0.69 mm d^{-1}. These relationships were highly statistically significant ($p < 0.001$). Contrary, the CWSI-based ETa algorithm exhibited substantially weaker performance, with a low correlation coefficient ($r = 0.42$) and a very low R^2 value of 0.18. Furthermore, CWSI produced the highest prediction errors, with an RMSE of 1.91 mm d^{-1} and MAE of 1.40 mm d^{-1}, indicating limited accuracy in estimating ET. The SEBS algorithm demonstrated moderately strong performance with a correlation coefficient of 0.86 and R^2 of 0.75. However, the model produced higher error values, with an RMSE of 1.07 mm d^{-1} and MAE of 0.87 mm d^{-1}, indicating greater variability in prediction errors compared to SEBAL and VI. The standard error (SE) of 1.12 mm d^{-1} further reflects this variability. Nevertheless, the correlations remained statistically significant ($p < 0.001$). The Bias analysis indicated that SEBAL and SEBS slightly overestimated lysimeter ETa, with average biases of 0.33 mm d^{-1} and 0.52 mm d^{-1} respectively, whereas the VI model slightly underestimated ETa, with a mean bias of approximately −0.12 mm d^{-1}.

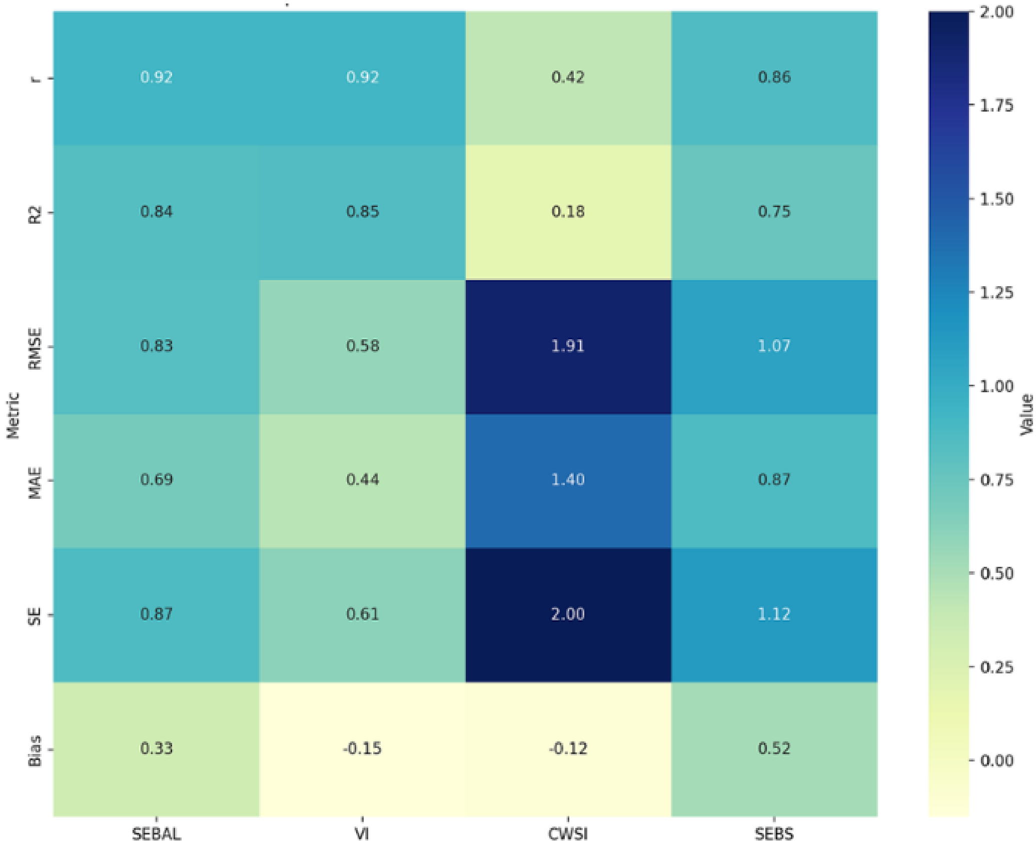

Figure 7. Evaluation best performing algorithms at the experimental site.

3.4~~2~~ The spatial distribution of ETa based on the four remote sensing algorithms

Figure 8~~5~~ presents the spatial distribution of ETa variation across the irrigation scheme for the period between 9th September 2019 and 27th October 2019. The spatial distribution maps are at a 30-meter spatial resolution. The maps shown are based on four remote sensing algorithms used to estimate daily ETa on the satellite pass days when the Landsat 8 images were free of clouds. On all three dates, ETa estimates show variability due to changes in environmental conditions like temperature, radiation, and vegetation activity. ETa values tend to increase toward the later date (October 27), especially with SEBAL, VI-ETa and SEBS, reflecting seasonal dynamics or crop growth. High ETa values (red regions) concentrated in areas with dense vegetation or high soil moisture. Low ETa values (green regions) are in regions with less vegetation or water stress. SEBAL and SEBS consistently estimate higher ETa values compared to CWSI and VI. The differences between algorithms highlight the variability in their sensitivity to input parameters like vegetation indices, surface temperature and energy balance terms. These maps provided ETa evaluation pixels at different station locations within the irrigation scheme. The estimates of ETa by SEBS, SEBAL and VI-based were comparable in most cases, while the CWSI estimates were mostly lower or extremely high in certain cases. The VI-based ETa had a minimum of 0 mm d^{-1} which was a result of bare soil pixels which are uncaptured by vegetation indices when estimating ETa. The spatial distribution maps aided in providing correlation pixels for the evaluation. More maps which demonstrate the spatial distribution of ETa across the irrigation scheme are in Figures (S2) - (S6).

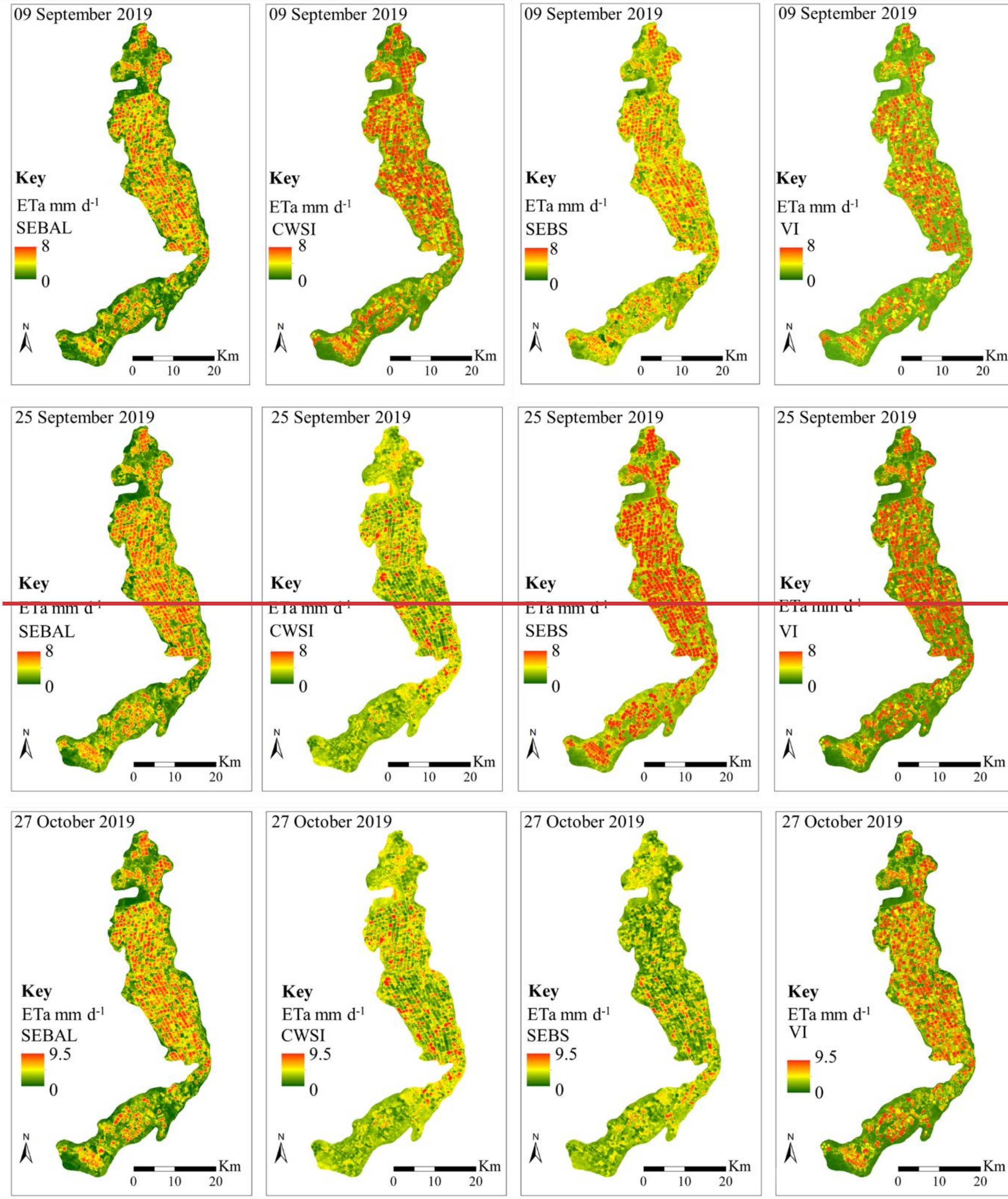
09 September 2019
Key
ETa mm d-1
SEBAL
8
0
N
Km
0 10 20
09 September 2019
Key
ETa mm d-1
CWSI
8
0
N
Km
0 10 20
09 September 2019
Key
ETa mm d-1
SEBS
8
0
N
Km
0 10 20
09 September 2019
Key
ETa mm d-1
VI
8
0
N
Km
0 10 20
25 September 2019
Key
ETa mm d-1
SEBAL
8
0
N
Km
0 10 20
25 September 2019
Key
ETa mm d-1
CWSI
8
0
N
Km
0 10 20
25 September 2019
Key
ETa mm d-1
SEBS
8
0
N
Km
0 10 20
25 September 2019
Key
ETa mm d-1
VI
8
0
N
Km
0 10 20
27 October 2019
Key
ETa mm d-1
SEBAL
9.5
0
N
Km
0 10 20
27 October 2019
Key
ETa mm d-1
CWSI
9.5
0
N
Km
0 10 20
27 October 2019
Key
ETa mm d-1
SEBS
9.5
0
N
Km
0 10 20
27 October 2019
Key
ETa mm d-1
VI
9.5
0
N
Km
0 10 20

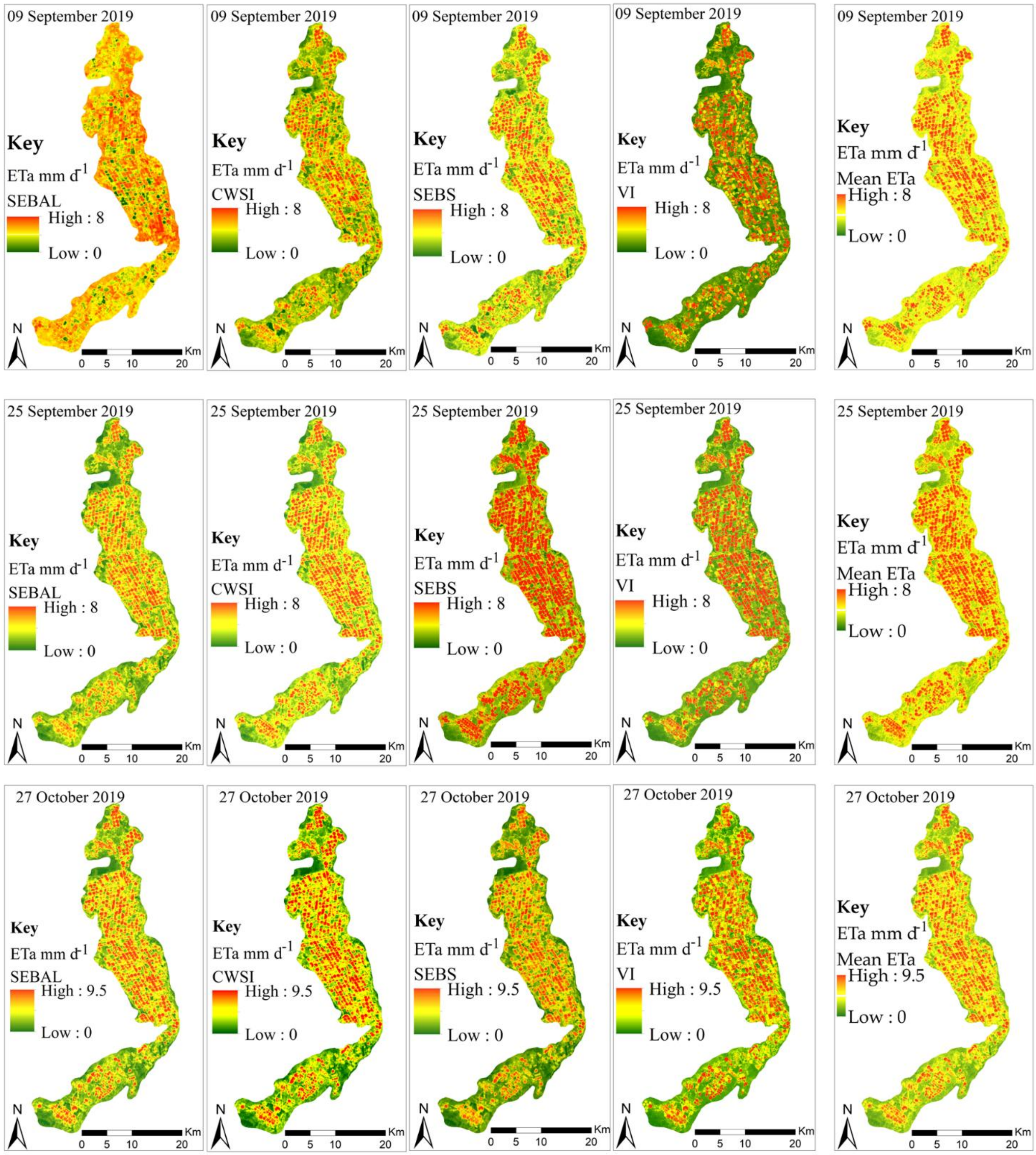

Figure ~~5~~8. An example of the **spatial distribution of ETa within Vaalharts irrigation scheme estimated by SEBAL, CWSI, SEBS and VI-based algorithms for the 9th of September 2019 to 27th October 2019.**

~~3.3 Evapotranspiration variability across different seasons and algorithms at the field scale~~experimental site

~~Figure 6 (a–d) presents the temporal trends between lysimeter ETa and ETa estimated using four algorithms at the field level. Figure 6–a shows the variations between lysimeter ETa and VI-ETa across the cropping seasons. The graphs indicate that, on most days, lysimeter ETa closely matched VI-ETa, with only slight underestimations and overestimations on some days. Overall, the differences were minimal.~~ SEBAL had the lowest average MAE of 0.46 mm d^{-1} across the four validation sites, compared to 0.52 mm d^{-1} for the VI-based ETa and 1.17 mm d^{-1} for SEBS. ~~Figure 6–b compares lysimeter ETa with SEBAL algorithm estimates. Both methods exhibited similar trends, with SEBAL estimates increasing and decreasing in tandem with lysimeter ETa. Throughout the cropping seasons, both methods captured ETa fluxes similarly. However, SEBAL tended to overestimate ETa on most days, with evident overestimations on days of the year (DOY) 31, 130, 207, 287, and 113, and slight underestimations around DOY 320.~~ Across the four validation stations, SEBAL exhibited an average bias of approximately 0.22 mm d^{-1}, indicating a slight tendency to overestimate ETa. In comparison, VI-based ETa had a slightly higher average bias of 0.26 mm d^{-1}, while SEBS showed a more pronounced overestimation bias of 0.89 mm d^{-1}. ~~Figure 6–c illustrates the relationship between lysimeter ETa and CWSI–ETa. Unlike the other algorithms, CWSI–ETa showed significant fluxes~~high variability ~~on most days, with values often surpassing those of lysimeter ETa. The lysimeter ETa displayed smoother variability compared to the more fluctuating CWSI–ETa values. Figure 6–d shows that SEBS ETa estimates closely tracked lysimeter ETa values, like the SEBAL and VI-ETa estimates. The scatter plots between the models and lysimeter ETa values is shown in Figure (S17).~~

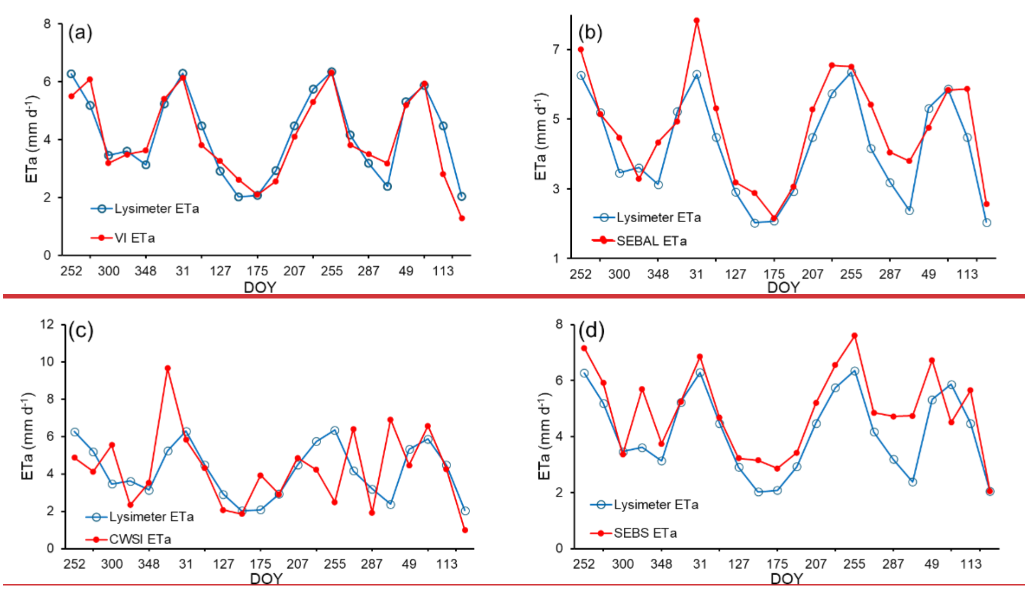

~~**Figure 6. Variability of lysimeter ETa and estimated ETa by VI ETa (a), SEBAL (b), CWSI ETa (c) and SEBS (d) algorithms.**~~

~~Figure 7 shows a comparison of the total ETa estimates from 2019 to 2021 which was a total of 22 days of cloud free Landsat 8 data across the four different algorithms: SEBAL, SEBS, VI-ETa, and CWSI-ETa against lysimeter-measured ETa in millimetres (mm). The total estimated ETa for each algorithm is represented by a bar in the corresponding colour. The lysimeter data acts as a benchmark of ETa, and differences in bar heights demonstrates how closely each algorithm aligns with the measured ETa. This reflection provides insight into the accuracy and reliability of the algorithms in estimating ETa over the study period. The total ETa measured by the lysimeter which matches the evaluated Landsat 8 images was 91.63 mm while SEBAL had a closer reading with only 1.41 mm. VI-based ETa followed with 2.36 mm which was followed by the SEBS algorithm with 5.63 mm difference whereas the CWSI-based ETa algorithm had the biggest difference of 16.24 mm over the evaluated period. These findings demonstrate the reliability of SEBAL, VI-based ETa and SEBS in accurately estimating ETa.~~

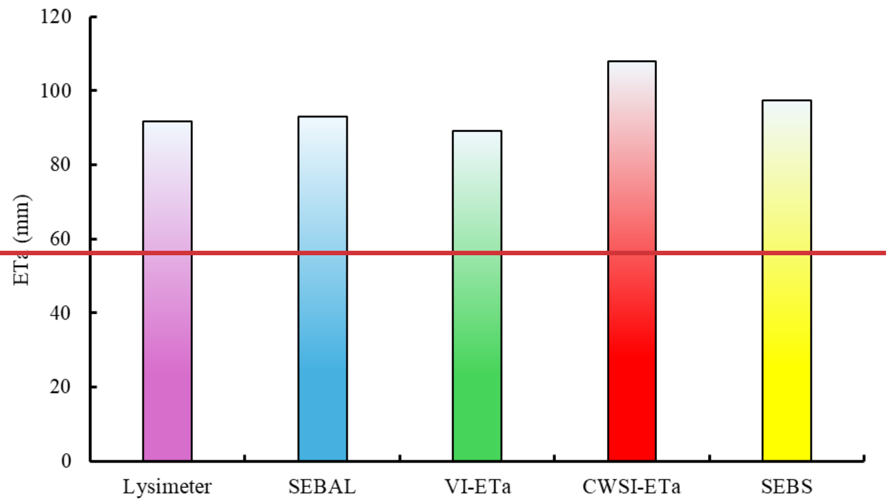

~~**Figure 7. Total lysimeter-measured and estimated ETa by SEBAL (blue), VI-ETa (green), CWSI (red) and SEBS (yellow) during the study period.**~~

~~**3.3.1 Summary of evaluation metrics for the four algorithms against the smart lysimeter at fieldarm scale**~~

~~The evaluation of SEBAL, VI, CWSI and SEBS ETa algorithms against the lysimeter measured ETa using statistical metrics shows significant differences in their performance as indicated on Fig.87. The SEBAL and VI algorithms demonstrate strong correlations with measured lysimeter ETa values where both have achieved high correlation coefficient (0.92) and R^2 values of 0.84 and 0.85, respectively which indicates a strong linear relationship. These methods exhibit the lowest RMSE and MAE values, indicating higher accuracy, with average prediction errors of 0.83 mm d^{-1} and 0.58 mm d^{-1} for RMSE, and 0.69 mm d^{-1} and 0.44 mm d^{-1} for MAE. The results are highly statistically significant, with p-values < 0.001. On the other hand, the CWSI-based ETa algorithm demonstrates a very low correlation coefficient of 0.42 with the R^2 value of 0.18, alongside higher RMSE of 1.91 mm d^{-1} and MAE of 1.40 mm d^{-1}, indicating poorer performance in both accuracy and explanation of variance.~~

~~The SEBS algorithm demonstrated a strong correlation with the correlation coefficient of 0.86 and a substantial R^2 of 0.75 with higher errors on RMSE of 1.07 and MAE of 0.87, mm d^{-1} and greater variability in prediction errors with SE of 1.12 and a highly statistically significant correlations with p value <0.001. The bias values indicate that SEBAL and SEBS generally overestimate the measured values by 0.33 mm d^{-1} and 0.52 mm d^{-1}, respectively, whereas VI tends to slightly underestimate them, with an average bias of approximately -0.12 mm d^{-1}. However, the SEBAL and VI are the most reliable methods with lower error rates, whereas CWSI has the least effectiveness in accurately predicting the measured lysimeter ETa values with R^2 of 0.18, RMSE of 1.91, MAE of 1.40 and a p value <0.05 showing the result are not statistically significant.~~

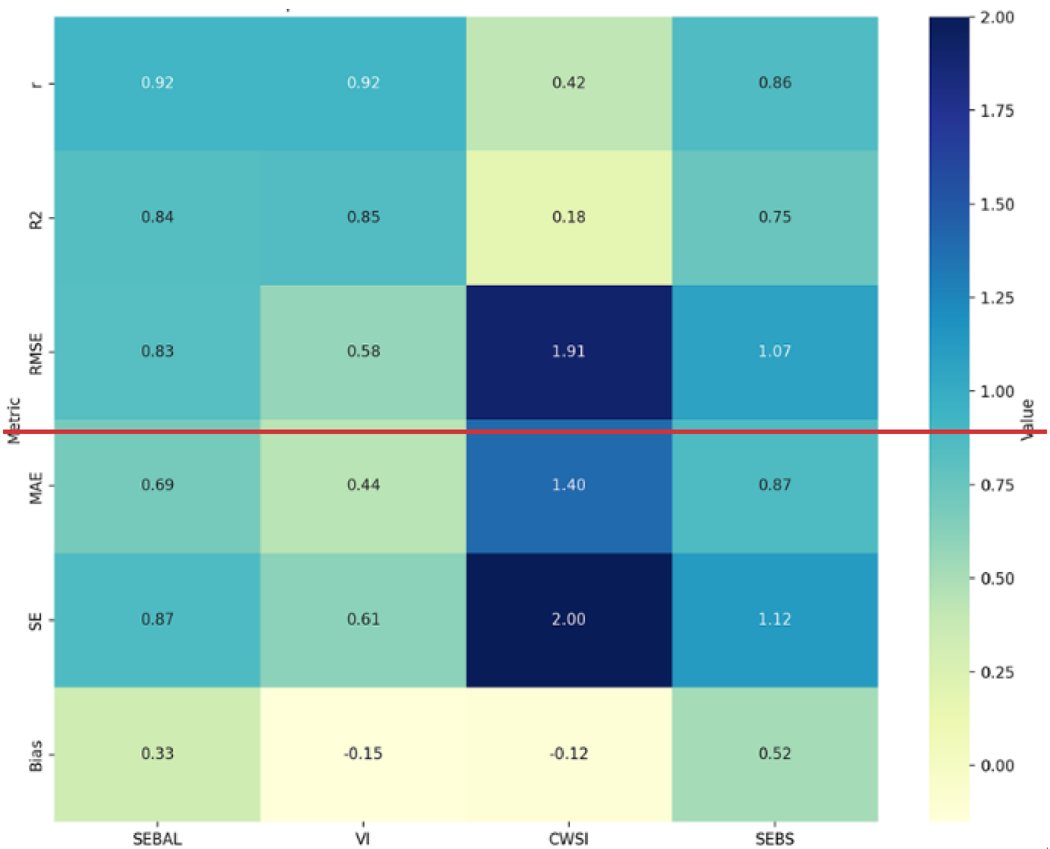

~~**Figure 87. Evaluation best performing algorithms at multi-stationsthe experimental site.**~~

3.5 Evaluation of algorithms across~~t~~ different locations with weather stations

The findings for the three algorithms which demonstrated promising performance at field level: SEBAL, SEBS, and VI-based reveal distinct differences in their accuracy and reliability across the validation weather station locations (Table 2). The SEBAL algorithm consistently demonstrates robust performance, with high correlation values, indicating a close match between its ETa estimates and extrapolated ETa data. The low error values reflect SEBAL's ability to make precise predictions with minimal bias, demonstrating its reliability across all sites. Although SEBS appears to be performing well, it shows more variability in its accuracy. Its correlation and determination coefficient values are slightly lower than SEBAL, while it exhibits higher prediction errors. This suggests that SEBS might be more sensitive to local environmental conditions or input data quality, leading to moderate discrepancies in its ETa estimates compared to the measured ETa values. The VI-based ETa performs better than SEBS in certain cases but not as consistently as SEBAL. It shows moderate correlation and determination coefficient values, with errors slightly higher than SEBAL but lower than SEBS. The bias values suggest that VI-based ETa might overestimate or underestimate ETa depending on the site, yet its statistical significance remains strong. SEBAL performs best across all sites with high correlation coefficients between 0.91 and 0.96, RMSE from 0.31 to 0.89 mm d-1. However, SEBS demonstrates moderate accuracy with higher RMSE values between 0.93–1.59 mm d-1. The VI-ETa was found to be better than SEBS in some cases but less consistent than SEBAL. CWSI demonstrated the worst performance across all evaluated sites as shown in Table S4.

Table 2. The statistical summary of performance of estimated daily ETa from SEBAL, VI, SEBS and CWSI based models at weather station sites.

Algorithm	**SEBAL ETa**				**SEBS ETa**				**VI ETa**			
Statistical Metric	SABBI	Tadcaster	Jankempdorp	Ganspan	SABBI	Tadcaster	Jankempdorp	Ganspan	SABBI	Tadcaster	Jankempdorp	Ganspan
r	0.93	0.94	0.96	0.91	0.89	0.81	0.90	0.78	0.90	0.80	0.90	0.86
R^2	0.87	0.88	0.92	0.83	0.80	0.66	0.81	0.61	0.82	0.63	0.80	0.73
RMSE	0.31	0.89	0.53	0.47	1.31	1.48	0.93	1.59	0.41	0.77	0.86	0.52
MAE	0.27	0.82	0.38	0.36	1.21	1.29	0.77	1.41	0.32	0.54	0.74	0.47
SE	0.10	0.31	0.19	0.17	0.17	0.52	0.33	0.56	0.12	0.27	0.31	0.19
Bias	0.01	0.70	0.26	-0.09	1.10	0.95	0.61	0.90	0.08	0.39	0.54	0.02
P value	<0.001	<0.001	<0.001	<0.001	<0.001	<0.001	<0.001	<0.001	<0.001	<0.001	<0.001	<0.001

Figure 9 demonstrates the scatter plots between ETa by each algorithm compared to extrapolated ETa on weather stations. The points displayed on each plot indicates the degree of correlation between the two sets of ETa values with those points along the line showing high correlations while those far apart indicates low correlations. The figure displays a series of scatter plots derived from the relationship between ETa estimated by each better performing algorithm and values of ETa extrapolated from lysimeter measurements with weather station measurements. The slope and alignment of the regression lines relative to the data points provide insight into the performance of each algorithm. The SEBAL approach shows regression lines closely aligned with the data, indicating strong agreement and a reliable estimation of ETa values, while the SEBS method displays greater variability, with data points more widely dispersed around the regression lines, reflecting less precise predictions compared to SEBAL. However, VI exhibits moderate performance, with data points closer to the regression lines than SEBS but not as tightly clustered as SEBAL.

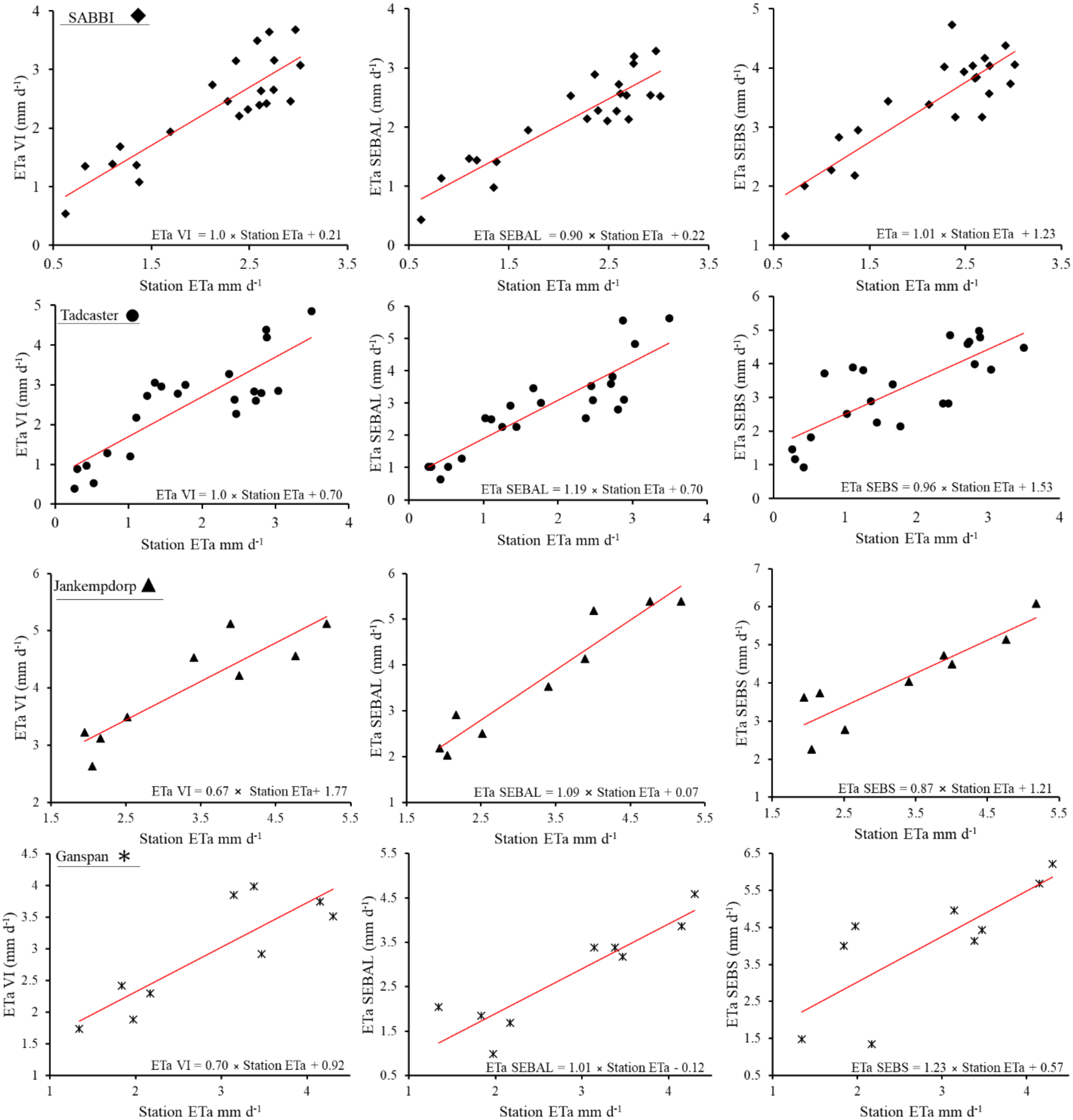

Figure 9. Scatter plots between ETa estimated using VI-ET, SEBAL and SEBS algorithms compared to extrapolated ETa on weather stations.

630

Section 3.6. Sensitivity analysis of different ETa estimation algorithms used.

The results demonstrated in Table (S3) shows a sensitivity analysis of the daily ETa estimates to ±5% and ±10% perturbations in three key input variables including T_air, Rn and NDVI. The findings show that SEBS is the most sensitive ETa algorithm to T_air and Rn where a ±10% change in T_air resulted in a 14.8% change in ETa, while Rn caused a 12.5% change. At~~h~~ the same time, the CWSI-ETa algorithm demonstrated a strong sensitivity to T_air with a 10.2% change at ±10% showing its reliance in the thermal band. Contrary, the SEBAL algorithm demonstrated a more balanced sensitivity, with both Rn and NDVI contributing equally to the model's uncertainty. For example, a ±10% change in Rn and NDVI led to 8.1% and 6.8% changes in ETa respectively. Moreover, the VI-ETa algorithm demonstrated the least sensitivity across all variables, with changes remaining below 6% even at the ±10% perturbation level.

4 Discussion

This study focused on the evaluation of multiple remote sensing-based ETa algorithms against lysimeter observations and extrapolated ETa values using weather stations. The main findings of this study were the observed differences in model performance. The findings indicate that the VI-based ETa algorithm produced the most accurate estimates, followed closely by SEBAL, while SEBS showed comparatively lower accuracy. In contrast, the CWSI-based ETa algorithm demonstrated limited reliability.

The study findings demonstrate the strengths and limitations of each algorithm as well as their implications for operational water management in irrigated agriculture. ~~This study focused on the evaluation of multiple remote sensing-based ETa algorithms against lysimeter observations and extrapolated ETa values using weather stations. The main findings of this study were the observed differences in model performance. The findings indicate that the VI-based ETa algorithm produced the most accurate estimates, followed closely by SEBAL, while SEBS showed comparatively lower accuracy. In contrast, the CWSI-based ETa algorithm demonstrated limited reliability.~~

~~The study findings demonstrate the strengths and limitations of each algorithm as well as their implications for operational water management in irrigated agriculture.~~ The determination of ETa using the VI-ETa approach demonstrates the utility of NDVI as a reliable proxy for vegetation dynamics and crop water use. The strong linear relationship observed between NDVI and Kc shows NDVI's ability to capture phenological changes and crop development under unstressed conditions. These findings align with those of Bausch and Neale (1987), Niu et al. (2020) and Pocas et al. 2020, who reported a good correlation between NDVI and Kc values. This consistency across studies emphasizes the strength of NDVI-based methods in agricultural water management. The ensemble Kc model, developed through an integration of season-specific Kc models, exhibited exceptional accuracy in aligned with ground-derived Kc values. The model's capacity to generalize Kc across diverse vegetation types and cropping seasons shows its potential for broad applicability in irrigated schemes like the Vaalharts scheme which is characterized by diverse crops and horticultural practices.

Validation of VI-ETa approach in estimating ETa against lysimeter measurements demonstrated its reliability with strong correlations and low error metrics. The slight underestimation of ETa, which reflected in a negative bias, suggests potential for fine-tuning the algorithm to account for localized environmental or crop-specific conditions. These results reflect the findings by Jarchow et al. (2022), who reported comparable accuracy in lysimeter-based validations. However, the VI-ETa approach also has limitations which were observed. For instance, the algorithm's dependence on vegetation surfaces restricts its utility in quantifying bare soil evaporation, necessitating complementary methods to address evaporation in sparsely vegetated areas. This limitation signifies an area for future refinement particularly in mixed land-use systems or early-season conditions with minimal vegetation cover. Beyond field-scale validations, the extrapolation of ETa estimates to broader spatial scales demonstrates the practicality of the algorithm for regional water resource management. The ability to estimate Kc values over large areas enhances precision irrigation planning and monitoring, this demonstrates critical needs in agricultural water management. The VI-ETa algorithm's performance in this study was enhanced by the ensemble Kc model which captures the diversity in vegetation phenology and water requirement which offers a reliable and scalable method for estimating crop water use. Although the NDVI–Kc models showed strong relationships across all seasons, we acknowledge that crop-specific differences in canopy architecture, rooting depth, and transpiration rates influence these regressions. The ensemble approach partially mitigates this variability, but future work could improve accuracy by building a crop-type stratified NDVI–Kc library to better capture the range of crops grown in the scheme.

The SEBAL algorithm demonstrated a strong performance in estimating ETa, as evidenced by its statistical indicators across the weather station locations. The ETa estimates in this study were extrapolated across the irrigation scheme using remote sensing algorithms parameterized with meteorological data from a weather station located within the experimental field. This approach assumes that atmospheric and surface conditions across the scheme are sufficiently homogeneous for the station data to be representative of the broader area. These assumptions are reasonable in the study area due to the relatively uniform topography, similar cropping patterns and consistent irrigation practices throughout the scheme. Moreover, the local variability in microclimate, soil moisture and crop conditions could influence ETa estimates at finer spatial scales. However, a slight positive bias indicates a tendency for overestimation. In instances where estimates from SEBAL are used for crop water requirements, the overestimation can be accounted for during irrigation scheduling to reduce the overuse of water. Despite the obtained minor overestimations on this study, SEBAL algorithm remains one of the most reliable algorithms for ETa estimation which provides a good balance between complexity and accuracy (Bastiaanssen, 2000). The performance aligns with some previous studies which applied SEBAL algorithm, for instance, Shoko et al. (2015) demonstrated SEBAL's efficacy in a South African context, where it achieved high accuracy using Landsat 8 and MODIS data validated against eddy covariance system measurements. They reported lower values being estimated using MODIS data with ETa difference compared to Landsat 8 estimates. Allen et al. (1998) validated SEBAL's estimates against lysimeter ETa measurements, confirming its suitability for watershed-scale applications. Although these comparisons affirm the reliability of SEBAL, they also highlight its adaptability across various environmental and spatial scales. The slight overestimation observed in this study may stem from assumptions inherent in SEBAL's parameterization such as surface albedo and aerodynamic resistance, which could vary under specific microclimatic conditions. Moreover, the resolution of the input satellite data plays a role; higher-resolution datasets, like those from Landsat 8, tend to improve estimation accuracy although it may still introduce minor discrepancies depending on land cover heterogeneity.

On the other hand, the CWSI-based ETa estimation showed the weakest performance among all algorithms evaluated, with weak statistical metrics. These findings suggest that CWSI-based method may not be suitable for precise ETa estimation in environments characterized by high variability in land use and water stress regimes. The poor performance of CWSI algorithm can be attributed to the method's reliance on capturing thermal dynamics which poses challenges, this is typically the case when using thermal data with coarse resolution such as the 90 m spatial resolution of Landsat 8 satellite. Katimbo et al. (2022) highlighted the sensitivity of CWSI to soil water depletion, particularly when levels drop below 80% of field capacity. This sensitivity becomes problematic in arid environments where moisture deficits are pronounced and soil moisture fluctuates significantly, leading to inaccuracies in ETa estimation. Furthermore, studies by Liu et al. (2022) and Boyaci et al. (2024) have demonstrated that the performance of CWSI is influenced by factors including crop type, environmental conditions, and calibration of temperature measurements. These factors contribute to variability in how well CWSI reflects ETa rates. In this study, such variability may have limited the method's effectiveness in capturing the dynamic water stress conditions experienced by crops. While the CWSI provides a temperature-based indication of water stress, it does not fully account for other critical factors influencing ET, such as atmospheric evaporative demand and plant physiological responses. This limitation, as discussed by Liu et al. (2022), may explain the observed discrepancies and demonstrates the need for caution when applying CWSI in areas where environmental and crop conditions vary significantly.

The SEBS algorithm showed a strong potential in estimating ETa at the field level when compared against smart field weighing lysimeter measurements. However, its performance varied across different validation sites, with the lowest correlation observed at Ganspan validation site. Despite this variability, the results suggest that SEBS estimates generally maintain a strong linear relationship with ground-based measurements and extrapolated ETa values, confirming the algorithm's reliability under specific conditions. Nevertheless, certain limitations of SEBS were evident. The algorithm exhibited higher errors compared to SEBAL with a tendency to overestimate ETa. This overestimation may reflect the algorithm's sensitivity to input parameters or specific environmental conditions, suggesting the need for calibration to improve its accuracy in heterogeneous settings such as the Vaalharts irrigation scheme. Similar observations have been reported in other studies. For example, McCabe and Wood (2006) and Dobriyal et al. (2012) noted overestimations in forested areas, while Rwasoka et al. (2011) observed daily overestimations in grasslands. The heterogeneous environment which comprised of pecan trees, natural vegetation, grass and diverse crops likely contributed to the observed overestimation. The shared thermal pixels between different land covers may have skewed heat flux estimates when different land covers exist in one pixel. Moreover, findings from South Africa's Gibson et al. (2011) and Gokool et al. (2018) affirms the influence of climatic conditions and validation methodologies on SEBS performance. Gibson et al. (2011) observed overestimations under wet conditions, while Gokool's study in a sub-humid sugarcane farm reported low accuracies associated with ground measurement uncertainties. These findings highlight the importance of using accurate devices like weighing lysimeters and higher-resolution Landsat data, as done in this study, to improve SEBS calibration and applicability.

The evaluation of these algorithms highlights their respective strengths and limitations in estimating ETa within a heterogeneous irrigation scheme. SEBAL, VI-ETa and SEBS demonstrated strong potential for water management applications, while CWSI-ETa requires further refinement to address its limitations. The role of input data spatial resolution and the challenges of extrapolating ETa through weather stations from lysimeter measurements are critical considerations for enhancing the accuracy and applicability of these models. For instance, based on the sensitivity analysis which was conducted in assessing the extrapolation based on meteorological data and remote sensing inputs, it was found that SEBS is highly sensitive to T_air and Rn with ETa deviations up to 14.8%. This outcome demonstrates that SEBS rely more on accurate meteorological data as input. Moreover, the CWSI-ETa showed moderate sensitivity to T_air, while the SEBAL algorithm exhibited a more balanced sensitivity across all the input variables. Weather stations and lysimeters provide point-based measurements, which might not capture the spatial dynamics across larger areas. This mismatch can result in over- or underestimation when scaling up. Errors in weather station data such as temperature, wind speed and humidity measurements can propagate when used to validate or calibrate ETa models for larger areas. Moreover, algorithms may struggle to accurately account for varying levels of water stress across regions, particularly in arid zones where rapid moisture changes occur. Furthermore, in this study, the CWSI was derived using a simplified, remote sensing-based approach in which the minimum and maximum differences between LST air temperature were used as proxies for the wet and dry reference limits, respectively. Although this method enables spatial estimation of crop water stress, we acknowledge that it deviates from the original formulation of the CWSI, where these limits are defined under fully transpiring and non-transpiring conditions. Consequently, the resulting CWSI values should be interpreted as relative indicators of crop stress rather than absolute measures.

Although the used lysimeter system was very useful in the development of the evaluation framework in estimating soil water dynamics several limitations were discovered. The used lysimeter represent a very small surface area, which may not always adequately capture the spatial variability present in a large area. Variations in soil properties, crop types, irrigation uniformity and microclimatic conditions across the field can lead to differences in ETa that are not reflected in a single-point measurement. Although efforts were made to ensure that soil and crop conditions inside the lysimeter matched those of the surrounding area, slight disturbances during installation and differences in root growth or soil structure may have influenced the measurements. The representativeness of the data is therefore dependent on how well these conditions were maintained. As a result, while the lysimeter provides localized measurements, caution should be exercised when extrapolating these results to field scale, particularly in heterogeneous cropping systems.

5 Conclusions

In this study four algorithms: SEBAL, SEBS, VI-ETa and CWSI-ETa were used to estimate ETa which was evaluated using a smart field weighing lysimeter measured ETa. The findings demonstrated that among the evaluated, SEBAL and VI-ETa demonstrated the best performance, with strong accuracy and reliability. SEBAL showed high accuracy at both farm and scheme scales, making it a valuable tool for ETa estimation and water management. Although the study was conducted within the Vaalharts irrigation scheme, algorithms like SEBAL and VI-ETa demonstrate strong potential for widespread application in regions with comparable cropping systems and water resource challenges. For instance, the strong correlation between NDVI and Kc demonstrates the universal applicability of NDVI-based approaches for monitoring crop water use in diverse agricultural settings. The SEBAL algorithm provided highly accurate ETa estimates when evaluated against the smart field weighing lysimeter data at the experimental site within the Vaalharts Irrigation Scheme. This was indicated by the high R^2 value > 0.90 and RMSE which was as low as 0.31 mm d-1, This shows that, SEBAL has the capability for capturing spatial and temporal ETa variability. These results indicates that SEBAL-derived ETa estimates may serve as a reliable biophysical input for informing irrigation scheduling in data-scarce. However, the distinctiveness of the results also highlights critical site-specific complexities. The observed algorithm performances, particularly the limitations of CWSI-ETa in arid zones, point to the necessity of adapting models to local climatic and environmental conditions. Variations in microclimate, crop type and irrigation practices across regions can influence the reliability and accuracy of ETa estimates. The findings of this study make emphasis on the importance of integrating high-resolution satellite data with ground-based measurements to improve ETa estimation accuracy. Although the findings align with global literature, regional or site-specific local validations remain essential to account for localized factors such as soil heterogeneity and mixed land-use systems. This is key considering the limitations of direct ETa measurements in most parts of South Africa. The focus on general principles and site-specific adaptations can provide a framework for scaling these approaches to other regions. Optical satellite data can be constrained by cloud cover, revisit frequency and limited soil moisture sensitivity. Therefore, integrating satellite ETa estimates with ground tools such as soil moisture sensors with practical farm management methods including mulching and crop protection strategies can enhance water management outcomes, ~~These~~these hybrid approaches can allow for a more localized, real-time decision-making that responds to climate variation and farm-specific conditions. The results of this study have important implications for extrapolating ETa estimates through weather station data. Since the extrapolated ETa relies heavily on the accuracy of meteorological data inputs, the algorithms with high input sensitivity such as SEBS and CWSI-ETa may propagate errors during spatial up-scaling. Importantly, the low sensitivity of VI-ETa supports its broader application in large-scale or data-scarce environments. The reliance on measurements from a very small, localized surface introduces uncertainty when representing larger fields with spatial variability in soils and crops. Therefore, future studies should consider the use of multiple measurement points or complementary methods to improve representativeness at the field scale. This study used a single measurement point due to single lysimeter system being the only available device

6 Suggestions for further research

Future research efforts should explore how ETa estimates can be embedded into decision support systems or irrigation advisory platforms that provide direct recommendations to farmers and water managers. Moreover, studies should assess whether the use of ETa-based tools leads to measurable improvements in water use efficiency, crop yield, or cost savings. At the same time, more field-level experiments where water use is measured can help in validating the real-world utility of ETa information. Research should also support the co-designing of ETa-based applications where end-users can trust and adopt them. There is a need for ETa data to be translated into forms that support irrigation management decisions. Given the lack of ETa data in Africa, it is critical to deploy advanced measuring tools such as eddy covariance systems and high-precision lysimeters with open-access policies to ensure a wide-scale evaluations of ETa algorithms. Future research efforts should consider formal uncertainty propagation when extrapolating ETa, especially for applications in water resource planning and irrigation scheduling.

7 Statements and Declarations

Funding: This study was funded by the Water Research Commission (WRC) of South Africa under the project: C2022_2023−00978 and the Agricultural Research Council (ARC) of South Africa under the crop estimate project: ISC01203000027.

Competing interests: Authors declare no personal or financial interests that has any influence on the quality of this work.

Author contributions: PER: conceptualization, data curation, formal analysis, investigation, methodology, software, validation, visualization, and writing – original draft preparation. MAM, EA, GC: conceptualization, funding acquisition, investigation, project administration, supervision, validation, and writing – original draft preparation.

Data availability: Data used and generated for this study are included in the article through links while some data is available on request.

References

Abbasi, N., Nouri, H., Didan, K., Barreto-Muñoz, A., Chavoshi Borujeni, S., Salemi, H., Opp, C., Siebert, S., and Nagler, P.: Estimating Actual Evapotranspiration over Croplands Using Vegetation Index Methods and Dynamic Harvested Area, Remote Sens., 13, 5167, https://doi.org/10.3390/rs13245167, 2021.

Abd Elbasit, M.A.M. and Ratshiedana, P.E., 2024. SMART FIELD WEIGHING LYSIMETER FOR VALIDATION OF SATELLITE-BASED EVAPOTRANSPIRATION UNDER ARID ENVIRONMENTS. WRC Report No. 3163/1/24. Available on: https://www.wrc.org.za: Accessed on: 03 February 2026.

Allen, R. G., Pereira, L. S., Raes, D., and Smith, M.: Crop Evapotranspiration-Guidelines for computing crop water requirements-FAO Irrigation and drainage paper 56, Fao Rome, 300, D05109, 1998.

Allen, R. G., Tasumi, M., and Trezza, R.: Satellite-Based Energy Balance for Mapping Evapotranspiration with Internalized Calibration (METRIC)—Model, J. Irrig. Drain. Eng., 133, 380–394, https://doi.org/10.1061/(ASCE)0733-9437(2007)133:4(380), 2007.

Annandale, J., Jovanovic, N., Benade, N. and Allen, R., 2002. Software for missing data error analysis of Penman-Monteith reference evapotranspiration. *Irrigation science*, *21*(2), pp.57-67.

Bastiaanssen, W. G. M., Menenti, M., Feddes, R. A., & Holtslag, A. A. M. (1998). A remote sensing surface energy balance algorithm for land (SEBAL): 1. Formulation. *Journal of Hydrology*, 212–213, 198–212. https://doi.org/10.1016/S0022-1694(98)00253-4

Bastiaanssen, W. G. M.: SEBAL-based sensible and latent heat fluxes in the irrigated Gediz Basin, Turkey, J. Hydrol., 229, 87–100, 2000.

Bastiaanssen, W. G. M., Noordman, E. J. M., Pelgrum, H., Davids, G., Thoreson, B. P., and Allen, R. G.: SEBAL Model with Remotely Sensed Data to Improve Water-Resources Management under Actual Field Conditions, J. Irrig. Drain. Eng., 131, 85–93, https://doi.org/10.1061/(ASCE)0733-9437(2005)131:1(85), 2005.

Bausch, W.C. and C.M.U. Neale. 1987. Crop coefficients derived from reflected canopy radiation: A concept. Transactions of the ASAE 30(3):703-709.

Blatchford, M. L., Mannaerts, C. M., Njuki, S. M., Nouri, H., Zeng, Y., Pelgrum, H., Wonink, S., and Karimi, P.: Evaluation of WAPOR V2 evapotranspiration products across Africa, Hydrol. Process., 34, 3200–3221, https://doi.org/10.1002/hyp.13791, 2020.

Boyaci, S., Kocięcka, J., Atilgan, A., Liberacki, D., Rolbiecki, R., Saltuk, B., and Stachowski, P.: Evaluation of Crop Water Stress Index (CWSI) for High Tunnel Greenhouse Tomatoes under Different Irrigation Levels, Atmosphere, 15, 205, https://doi.org/10.3390/atmos15020205, 2024.

Cai, W., Ullah, S., Yan, L. and Lin, Y., 2021. Remote sensing of ecosystem water use efficiency: a review of direct and indirect estimation methods. *Remote Sensing*, *13*(12), p.2393.

Chakouri, M., Lhissou, R., El Harti, A., Maimouni, S., and Adiri, Z. (2020). Assessment of the image-based atmospheric correction of multispectral satellite images for geological mapping in arid and semi-arid regions. Remote Sensing Applications: Society and Environment, 19, 100420. https://doi.org/10.1016/j.rsase.2020.100420

Chicco, D., Warrens, M. J., and Jurman, G.: The coefficient of determination R-squared is more informative than SMAPE, MAE, MAPE, MSE and RMSE in regression analysis evaluation, PeerJ Comput. Sci., 7, e623, https://doi.org/10.7717/peerj-cs.623, 2021.

Dalton, J.: Experimental essays, on the constitution of mixed gases; on the force of steam or vapour from water and other liquids in different temperatures, both in a Torricellian vacuum and in air; on evaporation; and on the expansion of elastic fluids by heat, No Title, 1802.

Djaman, K., Rudnick, D. R., Moukoumbi, Y. D., Sow, A., and Irmak, S.: Actual evapotranspiration and crop coefficients of irrigated lowland rice (Oryza sativa L.) under semiarid climate, 2019.

Djaman, K., Mohammed, A. T., and Koudahe, K.: Accuracy of Estimated Crop Evapotranspiration Using Locally Developed Crop Coefficients against Satellite-Derived Crop Evapotranspiration in a Semiarid Climate, Agronomy, 13, 1937, https://doi.org/10.3390/agronomy13071937, 2023.

Dobriyal, P., Qureshi, A., Badola, R., and Hussain, S. A.: A review of the methods available for estimating soil moisture and its implications for water resource management, J. Hydrol., 458–459, 110–117, https://doi.org/10.1016/j.jhydrol.2012.06.021, 2012.

Doležal, F., Hernandez-Gomis, R., Matula, S., Gulamov, M., Miháliková, M., and Khodjaev, S.: Actual Evapotranspiration of Unirrigated Grass in a Smart Field Lysimeter, Vadose Zone J., 17, 1–13, https://doi.org/10.2136/vzj2017.09.0173, 2018.

Du Plessis, A., 2023. *South Africa's water predicament: Freshwater's unceasing decline* (Vol. 101). Springer Nature.

Elfarkh, J., Simonneaux, V., Jarlan, L., Ezzahar, J., Boulet, G., Chakir, A., and Er-Raki, S.: Evapotranspiration estimates in a traditional irrigated area in semi-arid Mediterranean. Comparison of four remote sensing-based models, Agric. Water Manag., 270, 107728, https://doi.org/10.1016/j.agwat.2022.107728, 2022.

Gibson, L., Munch, Z., Carstens, M., and Conrad, J.: Remote sensing evapotranspiration (SEBS) evaluation using water balance, Water Research Commission, 2011.

Gibson, L., Jarmain, C., Su, Z., and Eckardt, F.: Review: Estimating evapotranspiration using remote sensing and the Surface Energy Balance System – A South African perspective, Water SA, 39, https://doi.org/10.4314/wsa.v39i4.5, 2013.

Glenn, E. P., Nagler, P. L., and Huete, A. R.: Vegetation Index Methods for Estimating Evapotranspiration by Remote Sensing, Surv. Geophys., 31, 531–555, https://doi.org/10.1007/s10712-010-9102-2, 2010.

Gokool, S., Riddell, E. S., Swemmer, A., Nippert, J. B., Raubenheimer, R., and Chetty, K. T.: Estimating groundwater contribution to transpiration using satellite-derived evapotranspiration estimates coupled with stable isotope analysis, J. Arid Environ., 152, 45–54, 2018.

Hodson, T. O.: Root-mean-square error (RMSE) or mean absolute error (MAE): when to use them or not, Geosci. Model Dev., 15, 5481–5487, https://doi.org/10.5194/gmd-15-5481-2022, 2022.

Hunsaker, D. J., Pinter, P. J., and Kimball, B. A.: Wheat basal crop coefficients determined by normalized difference vegetation index, Irrig. Sci., 24, 1–14, https://doi.org/10.1007/s00271-005-0001-0, 2005.

Ingrao, C., Strippoli, R., Lagioia, G., and Huisingh, D.: Water scarcity in agriculture: An overview of causes, impacts and approaches for reducing the risks, Heliyon, 9, e18507, https://doi.org/10.1016/j.heliyon.2023.e18507, 2023.

Jackson, R. D., Idso, S. B., Reginato, R. J., and Pinter, P. J.: Canopy temperature as a crop water stress indicator, Water Resour. Res., 17, 1133–1138, https://doi.org/10.1029/WR017i004p01133, 1981.

Jarchow, C. J., Waugh, W. J., and Nagler, P. L.: Calibration of an evapotranspiration algorithm in a semiarid sagebrush steppe using a 3-ha lysimeter and Landsat normalized difference vegetation index data, Ecohydrology, 15, e2413, https://doi.org/10.1002/eco.2413, 2022.

Jiang, L., Wu, H., Tao, J., Kimball, J. S., Alfieri, L., and Chen, X.: Satellite-Based Evapotranspiration in Hydrological Model Calibration, Remote Sens., 12, 428, https://doi.org/10.3390/rs12030428, 2020.

Katimbo, A., Rudnick, D. R., DeJonge, K. C., Lo, T. H., Qiao, X., Franz, T. E., Nakabuye, H. N., and Duan, J.: Crop water stress index computation approaches and their sensitivity to soil water dynamics, Agric. Water Manag., 266, 107575, https://doi.org/10.1016/j.agwat.2022.107575, 2022.

Li, X., Yang, Y., Zhou, X., Han, S., Li, H., Yang, Y., and Hao, X.: Accuracy evaluation of ET and its components from three remote sensing ET models and one process based hydrological model using ground measured eddy covariance and sap flow, J. Hydrol., 626, 130374, https://doi.org/10.1016/j.jhydrol.2023.130374, 2023.

Lian, T., Xin, X., Peng, Z., Li, F., Zhang, H., Yu, S., and Liu, H.: Estimating Evapotranspiration over Heterogeneous Surface with Sentinel-2 and Sentinel-3 Data: A Case Study in Heihe River Basin, Remote Sens., 14, 1349, https://doi.org/10.3390/rs14061349, 2022.

Liu, L., Gao, X., Ren, C., Cheng, X., Zhou, Y., Huang, H., Zhang, J., and Ba, Y.: Applicability of the crop water stress index based on canopy–air temperature differences for monitoring water status in a cork oak plantation, northern China, Agric. For. Meteorol., 327, 109226, https://doi.org/10.1016/j.agrformet.2022.109226, 2022.

Mabhaudhi, T., Nhamo, L. and Mpandeli, S., 2021. Enhancing crop water productivity under increasing water scarcity in South Africa. In Climate change science (pp. 1-18). Elsevier.

Maisela, R. J.: Realizing agricultural potential in land reform: The case of Vaalharts irrigation scheme in the Northern Cape Province, Thesis, University of the Western Cape, 2007.

McCabe, M. F. and Wood, E. F.: Scale influences on the remote estimation of evapotranspiration using multiple satellite sensors, Remote Sens. Environ., 105, 271–285, https://doi.org/10.1016/j.rse.2006.07.006, 2006.

Mckenzie, R. L., Paulin, K. J., Bodeker, G. E., Liley, J. B., and Sturman, A. P.: Cloud cover measured by satellite and from the ground: Relationship to UV radiation at the surface, Int. J. Remote Sens., 19, 2969–2985, https://doi.org/10.1080/014311698214370, 1998.

McNamara, I., Baez-Villanueva, O. M., Zomorodian, A., Ayyad, S., Zambrano-Bigiarini, M., Zaroug, M., Mersha, A., Nauditt, A., Mbuliro, M., Wamala, S., and Ribbe, L.: How well do gridded precipitation and actual evapotranspiration products represent the key water balance components in the Nile Basin? J. Hydrol. Reg. Stud., 37, 100884, https://doi.org/10.1016/j.ejrh.2021.100884, 2021.

Meijninger, W. and Jarmain, C.: Satellite-based annual evaporation estimates of invasive alien plant species and native vegetation in South Africa, Water SA, 40, 95, https://doi.org/10.4314/wsa.v40i1.12, 2014.

Meyer, A.: Concerning several relationships between climate and soil in Europe, Chem. Erde, 2, 209–347, 1926.

~~Mndela, Y., Ndou, N. and Nyamugama, A., 2023. Irrigation scheduling for small-scale crops based on crop water content patterns derived from UAV multispectral imagery. Sustainability, 15(15), p.12034.~~

Moeletsi, M.E., Walker, S. and Hamandawana, H., 2013. Comparison of the Hargreaves and Samani equation and the Thornthwaite equation for estimating dekadal evapotranspiration in the Free State Province, South Africa. Physics and Chemistry of the Earth, Parts a/b/c, 66, pp.4-15.

Moeletsi, M. E., Myeni, L., Kaempffer, L. C., Vermaak, D., de Nysschen, G., Henningse, C., Nel, I., and Rowswell, D.: Climate Dataset for South Africa by the Agricultural Research Council, Data, 7, 117, 2022.

Mu, Q., Zhao, M., and Running, S. W.: Improvements to a MODIS global terrestrial evapotranspiration algorithm, Remote Sens. Environ., 115, 1781–1800, 2011.

Mukiibi, A., Franke, A. C., and Steyn, J. M.: Determination of Crop Coefficients and Evapotranspiration of Potato in a Semi-Arid Climate Using Canopy State Variables and Satellite-Based NDVI, Remote Sens., 15, 4579, https://doi.org/10.3390/rs15184579, 2023.

Mulovhedzi, N. E., Araya, N. A., Mengistu, M. G., Fessehazion, M. K., Du Plooy, C. P., Araya, H. T., and Van der Laan, M.: Estimating evapotranspiration and determining crop coefficients of irrigated sweet potato (Ipomoea batatas) grown in a semi-arid climate, Agric. Water Manag., 233, 106099, 2020.

Nagler, P., Glenn, E., Nguyen, U., Scott, R., and Doody, T.: Estimating Riparian and Agricultural Actual Evapotranspiration by Reference Evapotranspiration and MODIS Enhanced Vegetation Index, Remote Sens., 5, 3849–3871, https://doi.org/10.3390/rs5083849, 2013.

Ncoyini, Z., Savage, M. J., and Strydom, S.: Limited access and use of climate information by small-scale sugarcane farmers in South Africa: A case study, Clim. Serv., 26, 100285, https://doi.org/10.1016/j.cliser.2022.100285, 2022.

Ndou, N. N., Palamuleni, L. G., and Ramoelo, A.: Modelling depth to groundwater level using SEBAL-based dry season potential evapotranspiration in the upper Molopo River Catchment, South Africa, Egypt. J. Remote Sens. Space Sci., 21, 237–248, https://doi.org/10.1016/j.ejrs.2017.08.003, 2018.

Niu, H., Hollenbeck, D., Zhao, T., Wang, D., and Chen, Y.: Evapotranspiration Estimation with Small UAVs in Precision Agriculture, Sensors, 20, 6427, https://doi.org/10.3390/s20226427, 2020.

Ojo, O. I.: Mapping and modeling of irrigation induced salinity of Vaalharts irrigation scheme in South Africa, PhD Thesis, Tshwane University of Technology, 2013.

Ojo, O. I., Ochieng, G. M., and Otieno, F. O. A.: Assessment of water logging and salinity problems in South Africa: an overview of Vaal Harts irrigation scheme, Water Soc., 153, 477–484, 2011.

Pandey, P. K., Dabral, P. P., and Pandey, V.: Evaluation of reference evapotranspiration methods for the northeastern region of India, Int. Soil Water Conserv. Res., 4, 52–63, https://doi.org/10.1016/j.iswcr.2016.02.003, 2016.

Peters, A., Nehls, T., Schonsky, H., and Wessolek, G.: Separating precipitation and evapotranspiration from noise–a new filter routine for high-resolution lysimeter data, Hydrol. Earth Syst. Sci., 18, 1189–1198, 2014.

Pôças, I., Calera, A., Campos, I. and Cunha, M., 2020. Remote sensing for estimating and mapping single and basal crop coefficients: A review on spectral vegetation indices approaches. *Agricultural Water Management*, 233, p.106081. https://doi.org/10.1016/j.agwat.2020.106081

Pretorius, W. M.: Vaalharts: environmental aspects of agricultural land and water use practices, PhD Thesis, North-West University, 2018.

Ramoelo, A., Majozi, N., Mathieu, R., Jovanovic, N., Nickless, A., and Dzikiti, S.: Validation of Global Evapotranspiration Product (MOD16) using Flux Tower Data in the African Savanna, South Africa, Remote Sens., 6, 7406–7423, https://doi.org/10.3390/rs6087406, 2014.

Ratshiedana, P. E.: Monitoring crop water use using unmanned aerial vehicle (UAV) and surface energy balance algorithms: a case study of Vaalharts Irrigation Scheme, Northern Cape Province, South Africa, 2022.

Raza, A., Al-Ansari, N., Hu, Y., Acharki, S., Vishwakarma, D. K., Aghelpour, P., Zubair, M., Wandolo, C. A., and Elbeltagi, A.: Misconceptions of Reference and Potential Evapotranspiration: A PRISMA-Guided Comprehensive Review, Hydrology, 9, 153, https://doi.org/10.3390/hydrology9090153, 2022.

Rosa, L., Chiarelli, D. D., Rulli, M. C., Dell'Angelo, J., and D'Odorico, P.: Global agricultural economic water scarcity, Sci. Adv., 6, eaaz6031, https://doi.org/10.1126/sciadv.aaz6031, 2020.

Rwasoka, D. T., Gumindoga, W., and Gwenzi, J.: Estimation of actual evapotranspiration using the Surface Energy Balance System (SEBS) algorithm in the Upper Manyame catchment in Zimbabwe, Phys. Chem. Earth Parts ABC, 36, 736–746, https://doi.org/10.1016/j.pce.2011.07.035, 2011.

Saha, S. K., Ahmmed, R., and Jahan, N.: Actual Evapotranspiration Estimation Using Remote Sensing: Comparison of Sebal and Metric Models, in: Water Management: A View from Multidisciplinary Perspectives, edited by: Tarekul Islam, G. M., Shampa, S., and Chowdhury, A. I. A., Springer International Publishing, Cham, 365–383, https://doi.org/10.1007/978-3-030-95722-3_18, 2022.

Sharma, B., Molden, D., and Cook, S.: Water use efficiency in agriculture: Measurement, current situation and trends, 2015.

Shoko, C., Clark, D., Mengistu, M., Dube, T., and Bulcock, H.: Effect of spatial resolution on remote sensing estimation of total evaporation in the uMngeni catchment, South Africa, J. Appl. Remote Sens., 9, 095997, https://doi.org/10.1117/1.JRS.9.095997, 2015.

Singels, A., Jarmain, C., Bastidas-Obando, E., Olivier, F., and Paraskevopoulos, A.: Monitoring water use efficiency of irrigated sugarcane production in Mpumalanga, South Africa, using SEBAL, Water SA, 44, https://doi.org/10.4314/wsa.v44i4.12, 2018.

Su, Z. (1999). The Surface Energy Balance System (SEBS) for estimation of turbulent heat fluxes. ITC Technical Note, No. 56. University of Twente, Faculty of Geoinformation Sciences and Earth Observation (ITC), Enschede, The Netherlands.

Su, Z.: The Surface Energy Balance System (SEBS) for estimation of turbulent heat fluxes, Hydrol. Earth Syst. Sci., 6, 85–100, https://doi.org/10.5194/hess-6-85-2002, 2002.

Tan, L., Zheng, K., Zhao, Q., and Wu, Y.: Evapotranspiration Estimation Using Remote Sensing Technology Based on a SEBAL Model in the Upper Reaches of the Huaihe River Basin, Atmosphere, 12, 1599, https://doi.org/10.3390/atmos12121599, 2021.

Tran, B. N., Van Der Kwast, J., Seyoum, S., Uijlenhoet, R., Jewitt, G., and Mul, M.: Uncertainty assessment of satellite remote-sensing-based evapotranspiration estimates: a systematic review of methods and gaps, Hydrol. Earth Syst. Sci., 27, 4505–4528, https://doi.org/10.5194/hess-27-4505-2023, 2023.

USGS: https://earthexplorer.usgs.gov/, 2022. Accessed: 04 February 2023

Verwey, P. and Vermeulen, P.: Influence of irrigation on the level, salinity and flow of groundwater at Vaalharts Irrigation Scheme, Water SA, 37, https://doi.org/10.4314/wsa.v37i2.65861, 2011.

Wang, Y., Hu, J., Li, R., Song, B., Hailemariam, M., Fu, Y., and Duan, J.: Increasing Cloud Coverage Deteriorates Evapotranspiration Estimating Accuracy from Satellite, Reanalysis and Land Surface Models Over East Asia, Geophys. Res. Lett., 50, e2022GL102706, https://doi.org/10.1029/2022GL102706, 2023.

Yan, C.: The Three-Temperature Model to Estimate Evapotranspiration and its Partitioning at Multiple Scales: A Review, Trans. ASABE, 59, 661–670, https://doi.org/10.13031/trans.59.11087, 2016.

Zamani Losgedaragh, S. and Rahimzadegan, M.: Evaluation of SEBS, SEBAL, and METRIC models in estimation of the evaporation from the freshwater lakes (Case study: Amirkabir dam, Iran), J. Hydrol., 561, 523–531, https://doi.org/10.1016/j.jhydrol.2018.04.025, 2018.